A variable kinematic shell formulation applied to thermal stress of laminated structures

A variable kinematic shell formulation applied to thermal stress of laminated structures

E. Carrera[1], S. Valvano[1]

(1) Department of Mechanical and Aerospace Engineering,
Politecnico di Torino, Turin, Italy

Keywords:
Variable-Kinematic, Equivalent-Single-Layer, Layer-Wise, Finite Element Method, Thermo-Mechanical, Heat Conduction Problem, Carrera Unified Formulation, Shell.

Author and address for Correspondence
Dr. Erasmo Carrera
Full Professor,
Department of Mechanical and Aerospace Engineering
Politecnico di Torino,
Corso Duca degli Abruzzi, 24,
10129 Torino, ITALY,
tel +39.011.546.6836, fax +39.011.564.6899
e.mail: erasmo.carrera@polito.it

Abstract

In this paper, the thermo-elastic static analysis of multilayered shell structure is performed using some advanced theories, obtained by expanding the unknown displacement variables along the thickness direction using Equivalent-Single-Layer (ESL) models, Layer-Wise (LW) models, and Variable-Kinematic models. The Variable-Kinematic models permit to reduce the computational cost of the analyses grouping some layers of the multilayered structure with ESL models and keeping the LW models in other zones of the multilayer. This model is here extended for the static analysis of uncoupled thermo-mechanical problems. The results obtained with the classical assumed linear temperature profile along the thickness of the shell are compared with those achieved with the calculated temperature profile solving the Fourier heat conduction equation. The used refined models are grouped in the Unified Formulation by Carrera (CUF), and they accurately describe the displacement field and the stress distributions along the thickness of the multilayered shell. The shell element has nine nodes, and the Mixed Interpolation of Tensorial Components (MITC) method is used to contrast the membrane and shear locking phenomenon. The governing equations are derived from the Principle of Virtual Displacement (PVD), and the Finite Element Method (FEM) is employed to solve them. Cross-ply plates and shells with simply-supported edges, subjected to bi-sinusoidal thermal load are analyzed. Various aspect ratios and radius to thickness ratios are considered. The results, obtained with different theories within CUF context, are compared with the elasticity solutions given in the literature. From the results, it is possible to conclude that the shell element based on the CUF is very efficient in the study of thermo-mechanical problems of composite structures. The Variable-Kinematic models combining the ESL with the LW models, permit to have a reduction of the computational costs, respect with the full LW models, preserving the accuracy of the results in localized layers.

Introduction

In the last years, an increasing amount of new structural materials, such as layered composite materials, have been used for many engineering applications. More complex scenarios, like structure subjected to severe high thermal gradients and cycling changes of temperature, are investigated. The continuous development of advanced materials, combining some properties such as high specific strength and stiffness, and nearly zero coefficient of thermal expansion in the fiber orientation, leads to increasingly complex structural designs that require careful analysis. The analysis of layered composite structures is complicated in practice. Anisotropy, complicating effects such as the C_z^0 - Requirements (zig-zag effects in the displacements and interlaminar continuity for the stresses), the couplings between in-plane and out-of-plane strains, are some of the issues to encounter. In most of the practical problems, the solution demands applications of approximated computational methods. An overview of several computational techniques for the analysis of laminated structures can be read in the review articles [1, 2, 3]. The Finite Element Method (FEM) has a predominant role among the computational techniques implemented for the analysis of layered structures. Studies involving the thermo-elastic behavior using classical or first-order theories are described by Kant and Khare [4] and Khdeir and Reddy [5]. In recent years, several higher-order two-dimensional models have been developed for such problems, which consider only an assumed temperature profile through the thickness. Among these, of particular interest is the higher-order model by Whu and Chen [6]. The same temperature profile is used by Khare et alii [7] to obtain a closed-form solution for the thermomechanical analysis of laminated and sandwich shells. Khdeir [8] and Khdeir et alii [9] assume a linear or constant temperature profile through the thickness. Barut et alii [10] analyze the nonlinear thermoelastic behavior of shells using the Finite Element Method, but the assigned temperature profile is linear. In the framework of the arbitrary distribution of temperature through the thickness, Miller et alii [11] and Dumir et alii [12] are noteworthy, in the first a classical shell theory for composite shells is given, the second remarks the importance of the

zig-zag form of displacements in the thermal analysis of composite shells. In the case of shells, further investigations were made by Hsu et alii [13] for both closed form and Finite Element method, and by Ding [14] for a weak formulation for the case of state equations including the boundary conditions.

A large variety of plate/shell finite element implementations of higher-order theories (HOT) has been proposed in the last twenty years literature. For multilayered structures, in literature, two kinds of models can be adopted: the Equivalent-Single-Layer (ESL) models, or the Layer-Wise (LW) models. For the ESL models, the variables are independent of the number of layers. Differently, the LW models permit to consider different sets of variables per each layer. In many cases the LW models are more accurate than ESL models, meanwhile LW theories are more expensive than ESL ones in terms of computational cost. A satisfactory thermal stress analysis is only possible if advanced and refined computational models are developed to approximate the stiffness matrix correctly, and if a correct thermal load is recognized. Sometimes the evaluation of a correct thermal load could be mandatory on any further evaluation for the computational models. In other words, a wrong thermal load invalidates the static response of plate and shell structures even when advanced computational models are employed.

In the last years, several efforts have been addressed to make the models more efficient. A possible way is to combine multiple models in the analysis of laminate problems; the issue is to maximize the accuracy keeping when it is possible a reduced computational cost. One of the simple types of multiple model methods, for composite laminates analysis, is the concept of selective ply grouping or sublaminates [15, 16, 17]. The approach consists of creating some local regions, identified by specific ply or plies, within which accurate stresses are desidered. The rest of the plies are identified as a global region or the domain part lying outside the local area. In literature, the local region is often modeled by using 3-D finite elements for each material plies, while the global region can be represented by 3-D finite elements grouped in one or more sublaminates. In the global region, the grouped sublaminates can be modeled with an ESL finite element model. The disadvantage of this approach is the use of the 3-D finite elements. Recently this technique of selective ply grouping or sublaminates has been employed

using only 2-D finite elements for both local region and global region. The authors of the present paper used a variable description in the thickness direction of the displacements, [18, 19]. The local region can be described with more accuracy by the use of LW models, meanwhile the global region can be represented by ESL models. Both ESL and LW models are described by the use of Legendre polynomials. The continuity of the primary variables between local and global region is immediately satisfied using the Legendre polynomials. In the work of Botshekanan Dehkordi et al. [20], a variable description in the thickness direction for the static analysis of sandwich plates was performed. That model was derived from the Reisnner-Mixed-Variational-Theorem (RMVT) to describe apriori the transverse shear and normal stresses. The transverse stresses were approximated through a mixed LW/ESL approach. The same mixed LW/ESL approach with RMVT was then used in [21] for nonlinear dynamic analysis of sandwich plates with flexible core and composite faces embedded with shape memory alloy wires.

In this work, the thermo-mechanical analysis of multilayered composite structures is performed with an improved shell finite element with a Variable-Kinematic model. It is based on the Carrera's Unified Formulation (CUF), which was developed by Carrera for multi-layered structures [22, 23, 24]. Based on CUF many works has been developed such as a fully coupled thermo-mechanical analysis applied to plate structure in [25]. Different type of thermal loads as distributed loads or localized in-plane distribution of temperature were considered in [26]. The importance of mixed theories for a correct prediction of transverse shear/normal stresses due to thermal loadings has been remarked in [27, 28]. Extension to Functionally Graded Materials (FGMs) has been done in [29]. An extension of the thermoelastic formulation to shells has been done in [30] and the Fourier heat conduction equation was employed for shell in [31]. The thermo-mechanical analysis of functionally graded shell is considered in [32].

In this paper, both Equivalent Single Layer (ESL) and Layer Wise (LW) theories contained in the CUF have been implemented in the shell finite element. A Variable-Kinematic model, obtained combining the ESL and LW models, is developed. The Mixed Interpolation of Tensorial Components (MITC)

method [33, 34, 35, 36] is used to contrast the membrane and shear locking. The governing equations for the thermo-mechanical uncoupled linear static analysis of composite structures are derived from the Principle of Virtual Displacement (PVD), to apply the finite element method. Cross-ply plates and cylindrical shells, and sandwich spherical shells with simply-supported edges and subjected to bi-sinusoidal thermal loads are analyzed. The results, obtained with the different models contained in the CUF, are compared with the exact solution given in the literature. This paper is organized as follows: an overview of higher-order and advanced shell theories developed within the CUF framework is given in Section . In Section a short outline of the different modeling approaches is given, and the explanation of the Variable-Kinematic model is drawn. Geometrical and constitutive relations for shells are presented in Section . Section gives a brief outline of the FEM approach, whereas, in Section , the governing equations in weak form for the thermo-mechanical uncoupled linear static analysis of composite structures are derived from the PVD. In Section a brief explanation of the use of the Fourier heat conduction equation for multilayered structures is given. In Section , the results obtained using the proposed CUF theories are discussed. Section is devoted to the conclusions.

Unified Formulation for Shells

In the literature, classical models are largely used when thin thickness and homogeneous properties are considered. Differently more sophisticated theories are needed, for the analysis of thick shells, to achieve sufficiently accurate results. As a general guideline, it is clear that the richer the kinematic field, the more accurate the 2D model becomes. Employing the Carrera Unified Formulation (CUF), each variable can be treated independently from the others, according to the required accuracy. With the CUF it is possible to expand each displacement variable at any desired order. This procedure becomes extremely useful when multifield problems are investigated such as thermoelastic and piezoelectric applications [27, 37, 38, 39]. According to the CUF [23, 40, 41], the displacement field can be written

as follows:

$$\begin{cases} u^k(\alpha,\beta,z) = F_0(z)\, u_0^k(\alpha,\beta) + F_1(z)\, u_1^k(\alpha,\beta) + ... + F_N(z)\, u_N^k(\alpha,\beta) \\ \\ v^k(\alpha,\beta,z) = F_0(z)\, v_0^k(\alpha,\beta) + F_1(z)\, v_1^k(\alpha,\beta) + ... + F_N(z)\, v_N^k(\alpha,\beta) \\ \\ w^k(\alpha,\beta,z) = F_0(z)\, w_0^k(\alpha,\beta) + F_1(z)\, w_1^k(\alpha,\beta) + ... + F_N(z)\, w_N^k(\alpha,\beta) \end{cases} \tag{1}$$

In compact form:

$$\boldsymbol{u}^k(\alpha,\beta,z) = F_s(z)\boldsymbol{u}_s^k(\alpha,\beta) \qquad \delta\boldsymbol{u}^k(\alpha,\beta,z) = F_\tau(z)\delta\boldsymbol{u}_\tau^k(\alpha,\beta) \qquad \tau,s = 0,1,...,N \tag{2}$$

where (α,β,z) is the general reference system (see Figure 1), the displacement vector $\boldsymbol{u} = \{u,v,w\}$ has its components expressed in this system. δ is the virtual variation associated to the virtual work and k identifies the layer. F_τ and F_s are the thickness functions depending only on z. τ and s are sum indexes and N is the number of terms of the expansion in the thickness direction assumed for the displacements. For the sake of clarity, the superscript k is omitted in the definition of the Legendre polynomials.

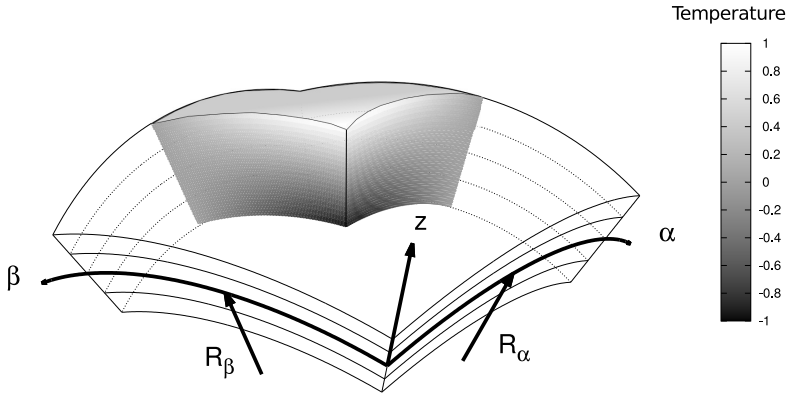

Figure 1: Reference system of the doubly-curved shell with a section of a temperature load.

Legendre-like polynomial expansions

In classical models, it is very common to employ a Taylor polynomial expansion, where the unknown variable are expressed in function of the midplane position of the shell. This limitation can be overcome

in several ways. A possible solution can be found employing the Legendre polynomials. They permit to express the unknown variables in function of the top and bottom position of a part of the shell thickness. In the case of Legendre-like polynomial expansion models, the displacements are defined as follows:

$$\boldsymbol{u} = F_0\,\boldsymbol{u}_0 + F_1\,\boldsymbol{u}_1 + F_r\,\boldsymbol{u}_r = F_s\,\boldsymbol{u}_s \qquad s = 0, 1, r \qquad r = 2, ..., N \tag{3}$$

$$F_0 = \frac{P_0 + P_1}{2} \qquad F_1 = \frac{P_0 - P_1}{2} \qquad F_r = P_r - P_{r-2} \tag{4}$$

in which $P_j = P_j(\zeta)$ is the Legendre polynomial of j-order defined in the ζ-domain: $-1 \leq \zeta \leq 1$. $P_0 = 1$, $P_1 = \zeta$, $P_2 = (3\zeta^2 - 1)/2$, $P_3 = (5\zeta^3 - 3\zeta)/2$, $P_4 = (35\zeta^4 - 30\zeta^2 + 3)/8$.

For the Layer-Wise (LW) models, the Legendre polynomials and the relative top and bottom position are defined for each layer.

Refined polynomials with Zig-Zag Function

Due to the intrinsic anisotropy of multilayered structures, the first derivative of the displacement variables in the z-direction is discontinuous. It is possible to reproduce the zig-zag effects in the framework of the ESL description by employing the Murakami theory. According to [42], a zig-zag term can be introduced into equation(3) as follows:

$$\boldsymbol{u} = F_0\,\boldsymbol{u}_0 + F_1\,\boldsymbol{u}_1 + F_r\,\boldsymbol{u}_r + (-1)^k \zeta_k \boldsymbol{u}_N^k \tag{5}$$

$$0 = top \qquad 1 = bottom \qquad r = 2, ..., N-1$$

Such theories are called zig-zag theories. The zig-zag function is defined in each layer k, where the adimensional term ζ_k takes value 1 and -1 at the top and the bottom respectively of each layer.

Modeling Approaches

The choice of the modeling approach is independent of the type of the used polynomials. In literature two different kinds of modeling approaches are usually used: the Equivalent Single Layer models, here named as ESL, and the Layer-Wise models, here indicated as LW. In this paper, a third modeling approach is taken into account. It is a variable kinematic model obtained as a combination of the ESL and LW models.

ESL models

In an ESL model, the stiffness matrix is obtained with a homogenization process of the properties of each layer by summing the contributions of each layer. This method leads to a model that has a set of variables that is assumed for the whole multilayer. In this work the ESL model is employed using Legendre polynomials. The ESL behavior of the primary variables along the thickness of the shell is shown in Figure 2.

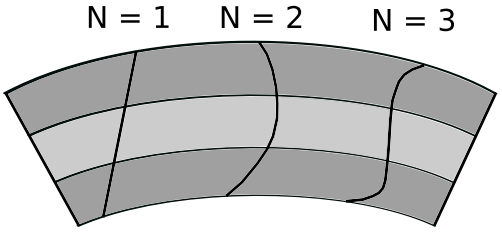

Figure 2: Equivalent-Single-Layer behavior of the primary variables along the thickness of the shell.

LW models

In an LW model, the homogenization is just conducted at the interface level. Different sets of variables per each layer are considered. In this work the LW model is employed using the Legendre polynomials. The Legendre polynomial F_0 and F_1 interpolate the displacements at the top (t) and bottom (b) position of the layer, respectively. The unknown variables at the top (t) and bottom (b) position are used to

impose the following compatibility conditions:

$$\boldsymbol{u}_t^k = \boldsymbol{u}_b^{k+1} \qquad k = 1, N_l - 1 \tag{6}$$

The LW behavior of the primary variables along the thickness of the shell is presented in Figure 3.

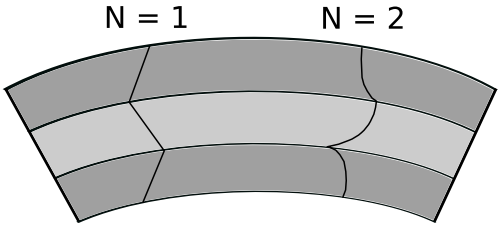

Figure 3: Layer-Wise behavior of the primary variables along the thickness of the shell.

Variable-Kinematics

In this paper, a different model is taken into account. This Variable-Kinematic model is obtained as a combination of the ESL and LW models. The combination of these two models is easily achieved using the Legendre polynomials. In multilayered structures, some layers can be modeled with a homogenization of the properties and modeled with an ESL assembling procedure, whereas for some layers the homogenization is conducted just at the interface level. This homogenization between the ESL and LW models is performed by the use of the Legendre polynomials. The Variable-Kinematic behavior of the primary variables along the thickness of the shell is shown in Figure 4. The Variable-Kinematic assembling, developed in the framework of the CUF, is very simple to integrate with few lines of programming. An overview of the assembling scheme of the ESL, LW and Variable-Kinematics approaches is given in Figure 5, where the concept of nucleus is anticipated from section .

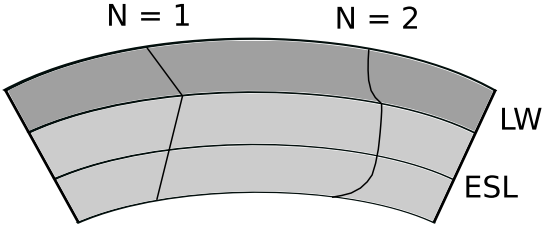

Figure 4: Variable-Kinematics behavior of the primary variables along the thickness of the shell.

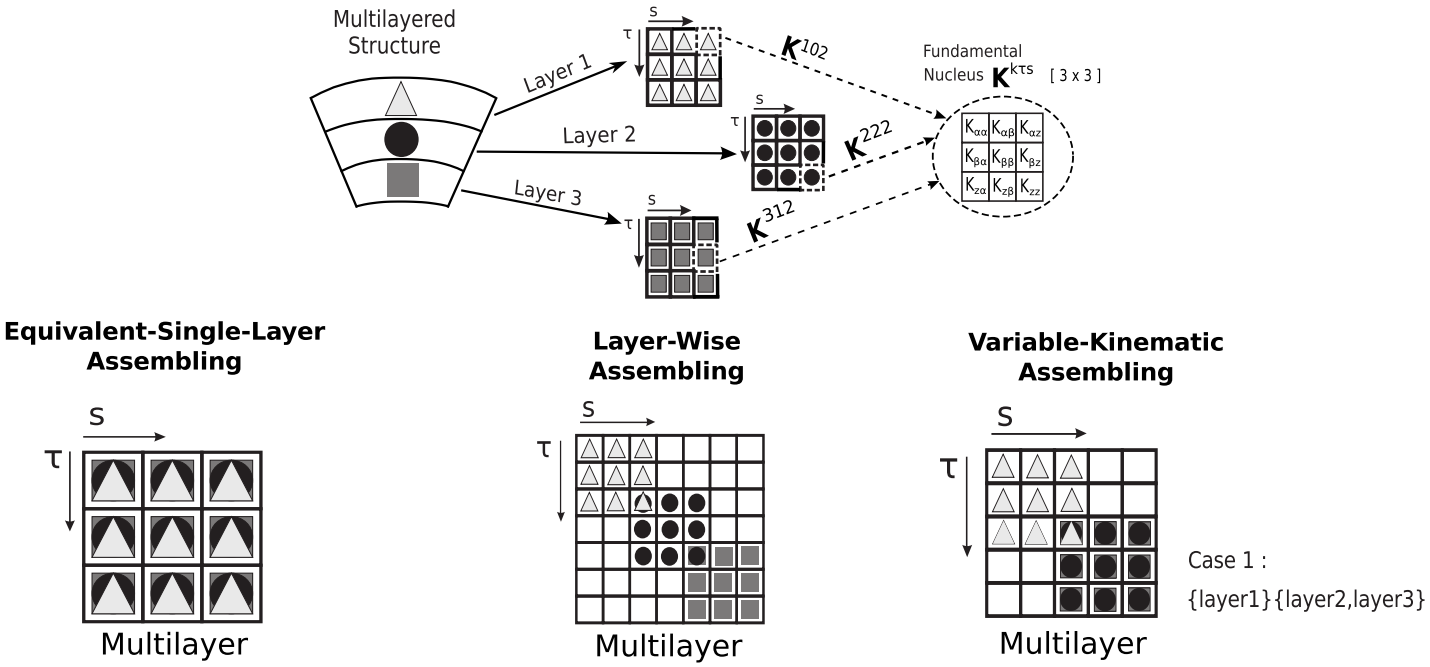

Figure 5: Overview of assembling scheme of the three different approaches.

Perliminaries for thermo-mechanical problems for shells

Shells are bi-dimensional structures in which one dimension (in general the thickness in the z direction) is negligible with respect to the other two dimensions. The reference system of the shell is indicated in Figure 1. By considering multilayered structures, the square of an infinitesimal linear segment in the layer, the associated infinitesimal area and volume are given by:

$$ds_k^2 = H_\alpha^{k\,2}\, d\alpha_k^2 + H_\beta^{k\,2}\, d\beta_k^2 + H_z^{k\,2}\, dz_k^2$$

$$d\Omega_k = H_\alpha^k H_\beta^k\, d\alpha_k\, d\beta_k \tag{7}$$

$$dV = H_\alpha^k\, H_\beta^k\, H_z^k\, d\alpha_k\, d\beta_k\, dz_k$$

where the metric coefficients are:

$$H_\alpha^k = A^k(1 + z_k/R_\alpha^k) \qquad H_\beta^k = B^k(1 + z_k/R_\beta^k) \qquad H_z^k = 1 \tag{8}$$

k denotes the k-layer of the multilayered shell; R^k_α and R^k_β are the principal radii of the midsurface of the layer k. A^k and B^k are the coefficients of the first fundamental form of Ω_k (Γ_k is the Ω_k boundary). In this paper, the attention has been restricted to shells with constant radii of curvature (cylindrical, spherical, toroidal geometries) for which $A^k = B^k = 1$. Details for shells are reported in [43]. The geometrical relations enable to express the in-plane $\boldsymbol{\epsilon}^k_p$ and out-plane $\boldsymbol{\epsilon}^k_n$ strains in terms of the displacement $\boldsymbol{u}$ for each layer k:

$$\begin{aligned} \boldsymbol{\epsilon}^k_p &= [\epsilon^k_{\alpha\alpha}, \epsilon^k_{\beta\beta}, \epsilon^k_{\alpha\beta}]^T = (\boldsymbol{D}^k_p + \boldsymbol{A}^k_p)\ \boldsymbol{u}^k \\ \boldsymbol{\epsilon}^k_n &= [\epsilon^k_{\alpha z}, \epsilon^k_{\beta z}, \epsilon^k_{zz}]^T = (\boldsymbol{D}^k_{n\Omega} + \boldsymbol{D}^k_{nz} - \boldsymbol{A}^k_n)\ \boldsymbol{u}^k \end{aligned} \tag{9}$$

The explicit form of the introduced arrays is:

$$\boldsymbol{D}^k_p = \begin{bmatrix} \frac{\partial_\alpha}{H^k_\alpha} & 0 & 0 \\ 0 & \frac{\partial_\beta}{H^k_\beta} & 0 \\ \frac{\partial_\beta}{H^k_\beta} & \frac{\partial_\alpha}{H^k_\alpha} & 0 \end{bmatrix} \quad \boldsymbol{D}^k_{n\Omega} = \begin{bmatrix} 0 & 0 & \frac{\partial_\alpha}{H^k_\alpha} \\ 0 & 0 & \frac{\partial_\beta}{H^k_\beta} \\ 0 & 0 & 0 \end{bmatrix} \quad \boldsymbol{D}^k_{nz} = \begin{bmatrix} \partial_z & 0 & 0 \\ 0 & \partial_z & 0 \\ 0 & 0 & \partial_z \end{bmatrix} \tag{10}$$

$$\boldsymbol{A}^k_p = \begin{bmatrix} 0 & 0 & \frac{1}{H^k_\alpha R^k_\alpha} \\ 0 & 0 & \frac{1}{H^k_\beta R^k_\beta} \\ 0 & 0 & 0 \end{bmatrix} \quad \boldsymbol{A}^k_n = \begin{bmatrix} \frac{1}{H^k_\alpha R^k_\alpha} & 0 & 0 \\ 0 & \frac{1}{H^k_\beta R^k_\beta} & 0 \\ 0 & 0 & 0 \end{bmatrix} \tag{11}$$

The definition of the constitutive equations that permit to express the stresses σ in terms of the strains ϵ is defined as follows:

$$\begin{aligned} \boldsymbol{\sigma}^k_p &= [\sigma^k_{\alpha\alpha}, \sigma^k_{\beta\beta}, \sigma^k_{\alpha\beta}] = \boldsymbol{\sigma}^k_{pd} - \boldsymbol{\sigma}^k_{pT} = \boldsymbol{C}^k_{pp}\ \boldsymbol{\epsilon}^k_p + \boldsymbol{C}^k_{pn}\ \boldsymbol{\epsilon}^k_n - \boldsymbol{\lambda}^k_p\ \theta^k \\ \boldsymbol{\sigma}^k_n &= [\sigma^k_{\alpha z}, \sigma^k_{\beta z}, \sigma^k_{zz}] = \boldsymbol{\sigma}^k_{nd} - \boldsymbol{\sigma}^k_{nT} = \boldsymbol{C}^k_{np}\ \boldsymbol{\epsilon}^k_p + \boldsymbol{C}^k_{nn}\ \boldsymbol{\epsilon}^k_n - \boldsymbol{\lambda}^k_n\ \theta^k \end{aligned} \tag{12}$$

where

$$\boldsymbol{C}_{pp}^k = \begin{bmatrix} C_{11}^k & C_{12}^k & C_{16}^k \\ C_{12}^k & C_{22}^k & C_{26}^k \\ C_{16}^k & C_{26}^k & C_{66}^k \end{bmatrix} \qquad \boldsymbol{C}_{pn}^k = \begin{bmatrix} 0 & 0 & C_{13}^k \\ 0 & 0 & C_{23}^k \\ 0 & 0 & C_{36}^k \end{bmatrix}$$
$$\boldsymbol{C}_{np}^k = \begin{bmatrix} 0 & 0 & 0 \\ 0 & 0 & 0 \\ C_{13}^k & C_{23}^k & C_{36}^k \end{bmatrix} \qquad \boldsymbol{C}_{nn}^k = \begin{bmatrix} C_{55}^k & C_{45}^k & 0 \\ C_{45}^k & C_{44}^k & 0 \\ 0 & 0 & C_{33}^k \end{bmatrix} \tag{13}$$

$$\boldsymbol{\lambda}_p^k = \boldsymbol{C}_{pp}^k\, \boldsymbol{\alpha}_p^k + \boldsymbol{C}_{pn}^k\, \boldsymbol{\alpha}_n^k$$
$$\boldsymbol{\lambda}_n^k = \boldsymbol{C}_{np}^k\, \boldsymbol{\alpha}_p^k + \boldsymbol{C}_{nn}^k\, \boldsymbol{\alpha}_n^k \tag{14}$$

$$\boldsymbol{\alpha}_p^k = \begin{bmatrix} \boldsymbol{\alpha}_1^k \\ \boldsymbol{\alpha}_2^k \\ 0 \end{bmatrix} \qquad \boldsymbol{\alpha}_n^k = \begin{bmatrix} 0 \\ 0 \\ \boldsymbol{\alpha}_3^k \end{bmatrix} \tag{15}$$

$$\boldsymbol{\lambda}_p^k = \begin{bmatrix} \boldsymbol{\lambda}_1^k \\ \boldsymbol{\lambda}_2^k \\ \boldsymbol{\lambda}_6^k \end{bmatrix} \qquad \boldsymbol{\lambda}_n^k = \begin{bmatrix} 0 \\ 0 \\ \boldsymbol{\lambda}_3^k \end{bmatrix} \tag{16}$$

The subscripts d and T mean mechanical and thermal contributions. For the sake of brevity, the expressions that relate the material coefficients C_{ij} to Young's moduli E_1, E_2, E_3, the shear moduli G_{12}, G_{13}, G_{23} and Poisson's ratios ν_{12}, ν_{13}, ν_{23}, ν_{21}, ν_{31}, ν_{32} are not given here, they can be found in [44]. α_{ij} are the thermal expansion coefficients, λ_{ij} are the coupling thermal coefficients and θ^k is the difference with a reference temperature.

Finite Element approximation

Independently from the choice of the thickness functions, a Finite Element Model (FEM) can be formulated. According to the common FEM approximation, the generalized displacements can be

expressed as a linear combination of the shape functions. Considering a 9-node finite element, the generalized displacement, and its variation are defined as follows:

$$\boldsymbol{u}_s = N_j \boldsymbol{u}_{s_j} \qquad \delta\boldsymbol{u}_\tau = N_i \delta\boldsymbol{u}_{\tau_i} \qquad \text{with} \quad i,j = 1,...,9 \tag{17}$$

where $\boldsymbol{u}_{s_j}$, $\delta\boldsymbol{u}_{\tau_i}$ are the nodal displacements and their virtual variations, and N_i, N_j are the Lagrangian shape functions defined in each node of the finite element. Substituing the compact form of the FEM approximation (Eq. (17)) in the generalized displacement expansion (Eq. (2)), one has:

$$\begin{aligned} \boldsymbol{u}(\alpha,\beta,z) &= F_s(z) N_j(\alpha,\beta) \boldsymbol{u}_{s_j} \qquad s = 0,1,...,N \\ \delta\boldsymbol{u}(\alpha,\beta,z) &= F_\tau(z) N_i(\alpha,\beta) \delta\boldsymbol{u}_{\tau_i} \quad \tau = 0,1,...,N \end{aligned} \tag{18}$$

Therefore, to overcome the numerical problems related to the shear locking, it is possible to use many computational procedures, such as reduced integration, selective integration [45], and the mixed interpolation of tensorial components (MITC) [33]. In this paper, a MITC technique is used to overcome the shear locking phenomenon, for more details see [39].

Governing FEM equations for uncoupled thermo-mechanical problems

The PVD for a multilayered shell structure reads:

$$\int_{\Omega_k}\int_{A_k} \left\{ \delta\boldsymbol{\epsilon}_p^{k\,T} \boldsymbol{\sigma}_p^k + \delta\boldsymbol{\epsilon}_n^{k\,T} \boldsymbol{\sigma}_n^k \right\} H_\alpha^k H_\beta^k \, d\Omega_k dz = \delta L_e \tag{19}$$

where Ω_k and A_k are the integration domains in the plane and the thickness direction, respectively. The left-hand side of the equation represents the variation of the internal work, while the right-hand side is the virtual variation of the external work. $\boldsymbol{\sigma}_p^k$ and $\boldsymbol{\sigma}_n^k$ contain the mechanical (d) and thermal (T) contributions, so:

$$\int_{\Omega_k}\int_{A_k} \left\{ \delta\boldsymbol{\epsilon}_p^{k\,T} \left(\boldsymbol{\sigma}_{pd}^k - \boldsymbol{\sigma}_{pT}^k \right) + \delta\boldsymbol{\epsilon}_n^{k\,T} \left(\boldsymbol{\sigma}_{nd}^k - \boldsymbol{\sigma}_{nT}^k \right) \right\} H_\alpha^k H_\beta^k \, d\Omega_k dz = \delta L_e \tag{20}$$

In this work no mechanical loads are applied to the shell structure, so the external work is null, except for the thermal stress contribution of the temperature distribution applied, so:

$$\int_{\Omega_k}\int_{A_k}\left\{\delta\boldsymbol{\epsilon}_p^{k\,T}\boldsymbol{\sigma}_{pd}^k+\delta\boldsymbol{\epsilon}_n^{k\,T}\boldsymbol{\sigma}_{nd}^k\right\}H_\alpha^k H_\beta^k\,d\Omega_k dz=\int_{\Omega_k}\int_{A_k}\left\{\delta\boldsymbol{\epsilon}_p^{k\,T}\boldsymbol{\sigma}_{pT}^k+\delta\boldsymbol{\epsilon}_n^{k\,T}\boldsymbol{\sigma}_{nT}^k\right\}H_\alpha^k H_\beta^k\,d\Omega_k dz \tag{21}$$

Substituting the constitutive equations (12), the geometrical relations written via the MITC method and applying the CUF (2 and the FEM approximation (17), one obtains the following governing equations:

$$\delta\boldsymbol{q}_{\tau i}^k:\boldsymbol{K}^{k\tau sij}\boldsymbol{q}_{sj}^k=\boldsymbol{\Theta}^{k\tau i} \tag{22}$$

where

$$\boldsymbol{K}^{k\tau sij}=\begin{bmatrix}K_{\alpha\alpha} & K_{\alpha\beta} & K_{\alpha z}\\ K_{\beta\alpha} & K_{\beta\beta} & K_{\beta z}\\ K_{z\alpha} & K_{z\beta} & K_{zz}\end{bmatrix}^{k\tau sij} \tag{23}$$

$$\boldsymbol{\Theta}^{k\tau i}=\begin{bmatrix}\Theta_\alpha\\ \Theta_\beta\\ \Theta_z\end{bmatrix}^{ksj} \tag{24}$$

where $\boldsymbol{K}^{k\tau sij}$ is a 3×3 matrix, called fundamental nucleus of the mechanical stiffness matrix, and its explicit expression is given in [46]. $\boldsymbol{\Theta}^{k\tau i}$ is a 3×1 matrix, called fundamental nucleus of the thermal load matrix, and its explicit expression is given in [37, 47]. The nucleus is the basic element from which the stiffness matrix and the thermal load matrix of the whole structure are computed. The fundamental nucleus is expanded on the indexes τ and s to obtain the stiffness matrix of each layer k. Then, the matrixes of each layer are assembled at the multi-layer level depending on the approach considered. $\boldsymbol{q}_{sj}^k$ and $\delta\boldsymbol{q}_{\tau i}^k$ are the nodal displacements and its variation respectively.

Fourier heat conduction equation in layered structures

The heat conduction problem is investigated by solving the Fourier heat conduction equation as described in [48] for the plate case. Here the solution is given for the shell case as proposed in [31]. If

the values of the temperature are known at the top and bottom surface of the shell, the temperature profile through the thickness can be considered in two different ways. The first method introduces an assumed profile $\hat{\theta}(z)$ that varies linearly from the top to the bottom as follows:

$$\hat{\theta}(z) = \theta_{bottom} + \frac{\theta_{top} - \theta_{bottom}}{h} * \left(z + \frac{h}{2}\right) \qquad z \in \left[\frac{-h}{2}\,;\,\frac{h}{2}\right] \tag{25}$$

Independetly by the number of considered layers the linear profile is always the same.

The second one computes $\hat{\theta}(z)$ by solving the Fourier heat conduction equation. In case of multi-layered structures, in general for the k^{th} homogeneous orthotropic layer, the differential Fourier equation of heat conduction reads:

$$\left(\frac{K_1^k}{(H_\alpha^k)^2}\right)\frac{\delta^2\theta}{\delta\alpha^2} + \left(\frac{K_2^k}{(H_\beta^k)^2}\right)\frac{\delta^2\theta}{\delta\beta^2} + \left(K_3^k\right)\frac{\delta^2\theta}{\delta z^2} = 0 \tag{26}$$

where K_1^k, K_2^k, K_3^k are the thermal conductivities coefficients in material coordinates $(1, 2, 3)$ for each orthotropic layer k and then rotated in the general curvilinear reference system (α, β, z). In case of multi-layered structures, continuity conditions for the temperature θ and the transverse normal heat flux q_z hold in the thickness direction at each k^{th} layer interface, reading:

$$\theta_t^k = \theta_b^{k+1} \qquad q_{zt}^k = q_{zb}^{k+1} \qquad for\, k = 1, ..., N_l - 1 \tag{27}$$

where N_l is the number of layers in the considered structure. The relationshp between the transverse heat flux and the temperature is given as:

$$q_z^k = K_3^k \frac{\delta\theta}{\delta z} \tag{28}$$

For the k^{th} layer of the shell structure it is supposed that K_1^k, K_2^k, K_3^k are constant because in each layer H_α^k, H_β^k are calculated. For each layer both governing equations and boundary conditions are satisfied by assuming the following temperature field:

$$\theta(\alpha, \beta, z) = f(z) \sin\left(\frac{m\pi\alpha}{a}\right) \sin\left(\frac{n\pi\beta}{b}\right) \tag{29}$$

where $f(z)$ is assumed as:

$$f(z) = \theta_0 \exp\left(s^k z\right) \tag{30}$$

where θ_0 is a constant and s^k a parameter. Substituting 29 in 26 and solving for s^k:

$$s^k_{1,2} = \pm\sqrt{\frac{\frac{K^k_1}{(H^k_\alpha)^2}\left(\frac{m\pi}{a}\right)^2 + \frac{K^k_2}{(H^k_\beta)^2}\left(\frac{n\pi}{b}\right)^2}{K^k_3}} \tag{31}$$

Therefore:

$$f(z) = \theta^k_{01}\exp\left(s^k_1 z\right) + \theta^k_{02}\exp\left(s^k_1 z\right) \text{ or}$$

$$f(z) = C^k_1\cosh\left(s^k_1 z\right) + C^k_2\sinh\left(s^k_1 z\right) \tag{32}$$

The solution for a layer k can be written as:

$$\theta_c(\alpha,\beta,z) = \theta^k = \left[C^k_1\cosh\left(s^k_1 z\right) + C^k_2\sinh\left(s^k_1 z\right)\right]\sin\left(\frac{m\pi\alpha}{a}\right)\sin\left(\frac{n\pi\beta}{b}\right) \tag{33}$$

wherein the coefficients C^k_1 and C^k_2 are constant for each layer k. In 32 for each layer k two unknowns (C^k_1 and C^k_2) remain. Therefore, if the number of layers is N_l, the number of unknowns is $(2\,N_l)$ and $(2\,N_l)$ equations to determine the unknowns are needed. The first two conditions are given by the temperature at the top and the bottom of the shell structure:

$$\begin{gathered} f(z_{bottom}) = \hat{\theta}_{bottom} = C^1_1\cosh\left(s^1_1 z_{bottom}\right) + C^1_2\sinh\left(s^1_1 z_{bottom}\right) \\ f(z_{top}) = \hat{\theta}_{top} = C^{N_l}_1\cosh\left(s^{N_l}_1 z_{top}\right) + C^{N_l}_2\sinh\left(s^{N_l}_1 z_{top}\right) \end{gathered} \tag{34}$$

Another $(N_l - 1)$ equations can be obtained from the continuity of temperature at each layer interface as follows:

$$C^k_1\cosh\left(s^k_1 z^k_t\right) + C^k_2\sinh\left(s^k_1 z^k_t\right) - C^{k+1}_1\cosh\left(s^{k+1}_1 z^{k+1}_b\right) - C^{k+1}_2\sinh\left(s^{k+1}_1 z^{k+1}_b\right) = 0 \tag{35}$$

and another $(N_l - 1)$ equations can be obtained from the continuity of heat flux through the interfaces as follows:

$$s_1^k K_3^k \left[C_1^k \sinh\left(s_1^k z_t^k\right) + C_2^k \cosh\left(s_1^k z_t^k\right) \right] - s_1^{k+1} K_3^{k+1} \left[C_1^{k+1} \sinh\left(s_1^{k+1} z_b^{k+1}\right) + C_2^{k+1} \cosh\left(s_1^{k+1} z_b^{k+1}\right) \right] = 0 \tag{36}$$

In 35 and 36 subscripts t and b indicate the top and bottom of each layer. Solving the system given by 34, 35 and 36 the $(2\,N_l)$ coefficients C_1^k and C_2^k are obtained. The temperature amplitude in the thickness shell direction is given by:

$$\hat{\theta}_c\left(z\right) = \hat{\theta}^k = C_1^k \cosh\left(s_1^k z\right) + C_2^k \sinh\left(s_1^k z\right) \qquad for\ k = 1, ..., N_l \tag{37}$$

Acronyms

Depending on the variables description and the number of terms N of the various expansion of kinematics plate theories can be obtained. A system of acronyms is given to denote these models. The first letter indicates the used approach in this work which is Equivalent Single Layer (E). The second letter indicates the type of polynomial adopted, (L) for the Legendre's polynomials. Sometimes a reference solution is given with a layer-wise approach, so the first letters become LW. The number N indicates the number of terms of the expansion used in the thickness direction. If the Navier analytical method is employed the subscript (a) is used. The letter Z is added if the zig-zag function of Murakami is employed. Therefore if the temperature profile is assumed linear the letters T_a can be added close to the model description, meanwhile if the temperature profile is calculated solving the Fourier heat conduction equation, it is indicated by the letters T_c.

Numerical results

To assess these theories the following reference problems have been considered:

- A three-layer square plate with lamination $[0°/90°/0°]$

- A ten-layer cylindrical shell panel with lamination $[0°/90°]_5$
- A sandwich composite spherical panel with lamination $[0°/90°/Core/90°/0°]$

Both of them are evaluated applying a thermal load with a bi-sinusoidal in-plane behavior:

$$\theta(\alpha,\beta,z) = \hat{\theta}(z)\sin\left(\frac{m\pi\alpha}{a}\right)\sin\left(\frac{n\pi\beta}{b}\right) \tag{38}$$

where $m = n = 1$. The three problems are briefly described in the following sections.

Three-layer plate

A three-layer cross-ply square plate, see Figure 6, with cross-ply composite layers with lamination $[0°/90°/0°]$ and simply-supported boundary condition is considered.

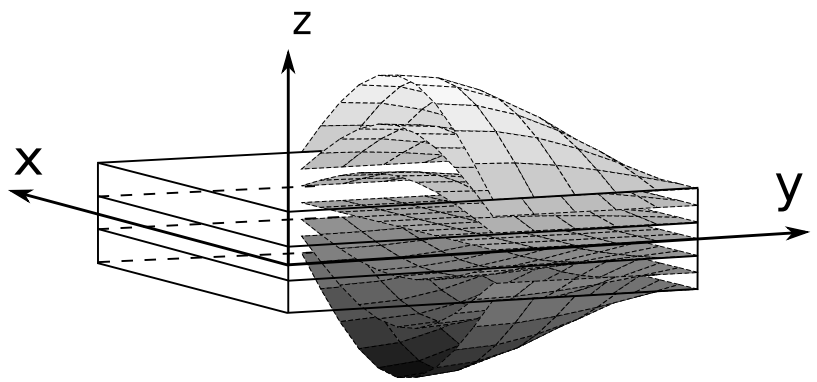

Figure 6: Reference system of the composite plate with section of thermal load applied.

The Carbon-Epoxy material constants of the plate are taken from [49, 37], the values are expressed in terms of ratios of the longitudinal and transversal fiber directional properties: $E_L/E_T = 25$; $G_{LT}/E_T = 0,5$; $G_{TT}/E_T = 0,2$; $\nu_{LT} = \nu_{TT} = 0,25$; $\frac{\alpha_T}{\alpha_L} = 1125,0$; $\frac{\mathcal{K}_L}{\mathcal{K}_T} = \frac{36,42}{0,96}$. The geometrical dimensions are: $a = b = 1,0$. The temperature boundary conditions are: $\hat{\theta}_{top} = +1,0$, $\hat{\theta}_{bottom} = -1,0$. The results are presented for different thickness ratios $a/h = 2; 100$, and the deflections and stresses are presented in the following dimensionless forms:

$$\hat{w} = \frac{w}{h\alpha_L\theta_0\left(\frac{a}{h}\right)^2} \qquad \hat{\sigma}_{i,j} = \frac{\sigma_{i,j}}{E_T\alpha_L\theta_0}$$

where the temperature gradient is $\theta_0 = 1$. A mesh grid of 32×32 elements is taken to ensure the convergence of the solution, see Table 1. The rate of convergence is invariant respect to the temperature profile.

Table 1: Convergence study. Composite three layered plate with thickness ratio $a/h = 100$. All the cases are computed with a $LW4$ model.

	Mesh	4×4	8×8	12×12	16×16	20×20	24×24	28×28	32×32	$3DExact$[49]
T_a	$\hat{w}$	10.274	10.261	10.260	10.260	10.260	10.260	10.260	10.260	10.26
	$\hat{\sigma}_{xx}$	1030.5	981.69	972.63	969.45	967.98	967.18	966.70	966.39	965.4
	$\hat{\sigma}_{xz}$	7.4509	7.1665	7.1150	7.0968	7.0883	7.0837	7.0809	7.0791	7.073
	$\hat{\sigma}_{zz}$	2.3686	0.1772	0.0379	0.0126	0.0056	0.0030	0.0019	0.0014	-0.1738×10^{-5}
T_c	$\hat{w}$	10.268	10.254	10.253	10.253	10.253	10.253	10.253	10.253	
	$\hat{\sigma}_{xx}$	1029.7	980.87	971.81	968.64	967.17	966.37	965.89	965.57	
	$\hat{\sigma}_{xz}$	7.4463	7.1621	7.1106	7.0924	7.0839	7.0793	7.0765	7.0747	
	$\hat{\sigma}_{zz}$	2.3652	0.1777	0.0378	0.0126	0.0055	0.0030	0.0019	0.0014	

Therefore a locking study has been performed evaluating different types of integration methods [45] for the same plate structure to prove that the element is locking free, see Table 2. The plate element with the MITC9 method ensures accuracy on both the transverse displacement and the stresses variables.

Table 2: Locking study. Composite three layered plate with thickness ratio $a/h = 100$. The $Temperature\,Assumed\,Linear$ and the $Temperature\,Calculated$ cases are computed with a mesh of 32×32 elements and with a $LW4$ model.

		Reduced	*Selective*	$MITC9$	$3DExact$[49]
T_a	$\hat{w}$	10.257	10.259	10.260	10.26
	$\hat{\sigma}_{xx}$	815.55	966.12	966.39	965.4
	$\hat{\sigma}_{xz}$	10.929	7.8184	7.0791	7.073
	$\hat{\sigma}_{zz}$	14.431	-0.0071	0.0014	-0.1738×10^{-5}
T_c	$\hat{w}$	10.251	10.253	10.253	
	$\hat{\sigma}_{xx}$	814.74	965.30	965.57	
	$\hat{\sigma}_{xz}$	10.924	7.8135	7.0747	
	$\hat{\sigma}_{zz}$	14.456	-0.0071	0.0014	

The description of the temperature profile along the thickness of the multilayered plate is given in Figure 7 for different aspect ratios a/h. It has to be noticed that for thin plates the temperature profile is almost linear or very close to it; differently for thick plates it is very important to use the calculated profile solving the Fourier heat conduction equation, the linear profile leads to relevant errors in the approximation of the temperature load, the temperature load is overestimated.

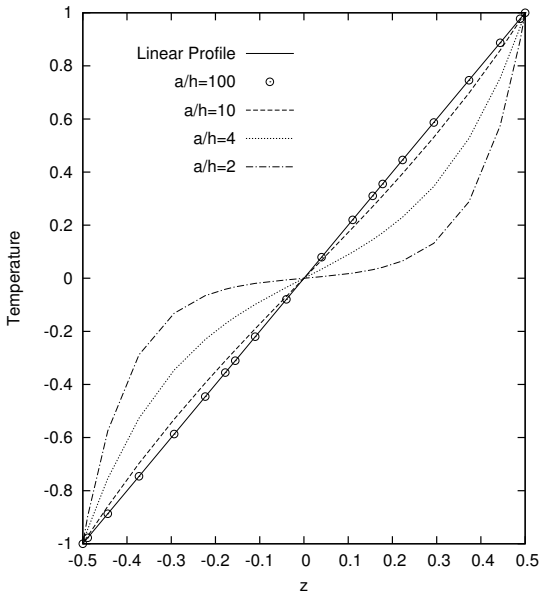

Figure 7: Three-layered plate. Temperature Profiles Comparison.

An assessment of the Legendre polynomials with a full ESL approach has been performed for the pure mechanical case in [18] for plates and in [19] for shells. All the results presented in [18, 19], for thick and thin plates and shells, show that the Legendre polynomials lead to the same results of the Taylor polynomials. The use of either polynomials is invariant respect to the solution accuracy.
Hereafter Legendre polynomials have been employed for the structure analyzes. Different Variable Kinematic models have been used to perform the analysis of the plate structures, see Figures 8. The acronyms have been modified adding a subscript to them, for the sake of clarity the list of subscripts is given below:

- $Case1 = \{layer1\}\,\{layer2, layer3\}$
- $Case2 = \{layer1, layer2\}\,\{layer3\}$

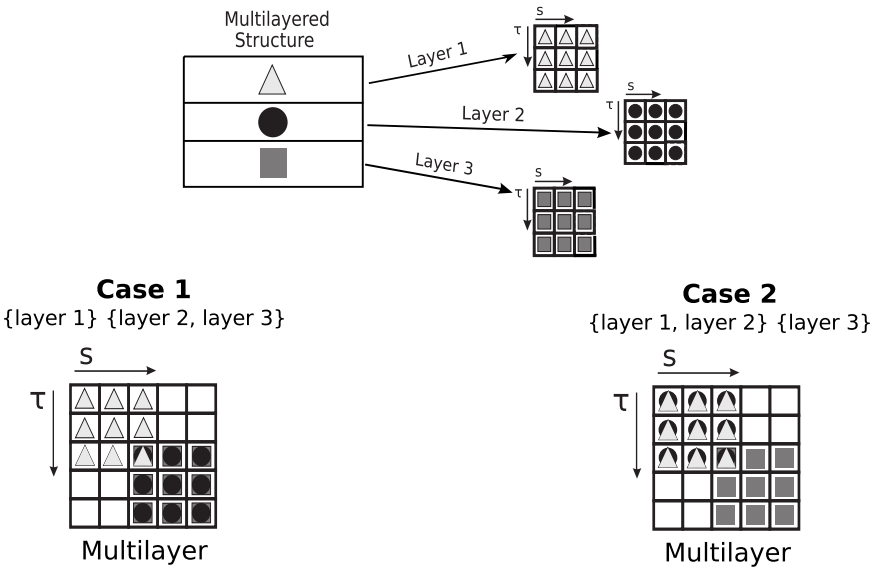

Figure 8: Variable Kinematic Cases. Compact example of assembling scheme.

The results are listed in Table 3. For the plate structures analysed the following considerations can be drawn:

- Regarding the transverse displacement w, for thin plates $a/h = 100$, the theories $EL4_{,Case1}$ and $EL4_{,Case2}$ lead a relevant improvement of the solution respect to the $EL4$ showing the same accuracy, see Figure 9a. The same comments can be drawn for both the temperature assumed linear cases T_a and for the temperature calculated via the Fourier heat conduction law T_c. For thick plates $a/h = 2$, the variable kinematic theories have the same accuracy of the full layer-wise and full equivalent-single-layer solutions, see Figure 9b. The maximum transverse displacement T_c case value is 49.53 % smaller than the T_a case, this relevant difference is due to temperature calculated profile T_c that permits to better describe the temperature load.

- For both the transverse shear stress σ_{xz}, see Figure 10a, and the transverse normal stress, see Figure 10b, the theories $EL4_{,Case1}$ and $EL4_{,Case2}$ improve the results respect to the $EL4$ theory only in the layer with a layer-wise description. It has to be noticed that no differences can be

appreciated between the temperature assumed linear cases T_a and the temperature calculated via the Fourier heat conduction law T_c cases.

- For the in-plane stress σ_{xx}, see Figures 11a, 11b, noticeable differences of the stress amplitude are present between the temperature assumed linear cases T_a and the temperature calculated profile T_c cases. The variable kinematic theories $EL4_{,Case1}$ and $EL4_{,Case2}$ improve the results respect to the $EL4$ theory only in the layer with a layer-wise description. It has to be noticed that the interlaminar continuity of the stress is reached in the temperature assumed cases T_a, but not in the calculated profile cases T_c.

Table 3: Three-layer composite plate with lamination $[0°/90°/0°]$. Mechanical variables described by Mono-models and Variable kinematic models for various aspect ratios a/h. Evaluation position for transverse displacement $\hat{w}(x,y,z) = \hat{w}(a/2, b/2, +h/2)$, in-plane stress $\hat{\sigma}_{xx}(x,y,z) = \hat{\sigma}_{xx}(a/2, b/2, +h/2)$, transverse shear stress $\hat{\sigma}_{xz}(x,y,z) = \hat{\sigma}_{xz}(0, b/2, +h/6)$, transverse normal stress $\hat{\sigma}_{zz}(x,y,z) = \hat{\sigma}_{zz}(a/2, b/2, +h/6)$.

T_a (Assumed Linear)									
	$a/h = 100$				$a/h = 2$				$DOFs$
	$\hat{w}$	$\hat{\sigma}_{xx}$	$\hat{\sigma}_{xz}$	$\hat{\sigma}_{zz}$	$\hat{w}$	$\hat{\sigma}_{xx}$	$\hat{\sigma}_{xz}$	$\hat{\sigma}_{zz}$	
$3DExact$[49]	10.26	965.4	7.073	-0.1738×10^{-5}	96.79	1390	63.92	-7.391	
$LW4_a$[37]	10.26	-	7.073	-	96.78	-	63.82	-	
$LW4$	10.260	966.39	7.0791	0.0014	96.783	1391.0	70.532	-5.9366	164775
$LW1$	10.915	893.99	1.8031	492.56	89.252	640.39	-3.9613	417.76	50700
$EL3Z$	10.260	966.39	7.0489	-0.0346	94.871	1279.6	110.16	-31.218	63375
$EL4$	10.253	966.28	10.365	-0.0074	98.215	1336.5	93.196	-12.266	63375
$EL3$	10.253	966.29	10.365	-0.0122	98.150	1335.3	93.208	-19.536	50700
$EL2$	10.231	964.60	4.5411	-0.0108	83.471	188.71	28.967	-17.038	38025
$EL1$	16.093	1240.6	7.9964	-487.39	42.714	164.03	114.24	-459.25	25350
$EL4_{Case\,1}$	10.258	966.36	7.0794	0.0014	96.679	1389.3	71.700	-5.9661	114075
$EL4_{Case\,2}$	10.258	966.38	10.466	-0.0063	97.009	1389.5	89.699	-11.812	114075
$EL3_{Case\,1}$	10.258	966.34	7.0789	0.0013	96.338	1376.4	43.807	-11.728	88725
$EL3_{Case\,2}$	10.258	966.37	9.9672	-0.0077	97.122	1331.9	99.761	-10.802	88725
$EL2_{Case\,1}$	10.258	966.33	8.0746	0.0031	94.629	1224.0	121.26	-11.109	63375
$EL2_{Case\,2}$	10.258	966.29	9.0002	-0.0176	95.508	1029.8	55.725	-20.599	63375
$EL1_{Case\,1}$	12.203	1042.9	2.4285	491.28	72.269	211.32	-12.328	435.51	38025
$EL1_{Case\,2}$	12.203	918.14	7.6641	0.0229	68.305	44.865	97.018	-40.574	38025

T_c (Calculated via Fourier Heat conduction Law)									
	$a/h = 100$				$a/h = 2$				$DOFs$
	$\hat{w}$	$\hat{\sigma}_{xx}$	$\hat{\sigma}_{xz}$	$\hat{\sigma}_{zz}$	$\hat{w}$	$\hat{\sigma}_{xx}$	$\hat{\sigma}_{xz}$	$\hat{\sigma}_{zz}$	
$LW4_a$[37]	10.25	-	7.069	-	49.09	-	30.11	-	
$LW4$	10.253	965.58	7.0747	0.0014	48.851	486.92	35.171	-13.392	164775
$LW1$	10.908	892.94	1.8018	492.57	44.174	33.733	-0.5026	344.19	50700
$EL3Z$	10.253	965.27	7.0443	0.3590	50.086	403.89	55.696	172.60	63375
$EL4$	10.246	965.47	10.360	-0.0074	49.301	410.42	59.850	-47.521	63375
$EL3$	10.246	965.17	10.360	0.3815	51.328	446.81	59.474	179.54	50700
$EL2$	10.224	963.49	4.5384	0.3829	40.880	-317.44	15.166	181.62	38025
$EL1$	16.083	1239.3	7.9915	-486.69	21.047	-329.45	56.660	-33.581	25350
$EL4_{Case\,1}$	10.252	965.55	7.0750	0.0014	48.741	484.86	35.799	-13.346	114075
$EL4_{Case\,2}$	10.252	965.56	10.460	-0.0064	48.830	446.19	59.176	-30.492	114075
$EL3_{Case\,1}$	10.251	965.51	7.0744	0.0371	48.805	454.55	17.787	85.001	88725
$EL3_{Case\,2}$	10.251	965.46	9.9617	-0.0077	49.179	395.76	62.223	-29.540	88725
$EL2_{Case\,1}$	10.251	965.39	8.0701	-0.3191	48.785	328.05	72.670	-224.56	63375
$EL2_{Case\,2}$	10.251	965.16	8.9953	0.3402	48.871	258.99	37.141	156.37	63375
$EL1_{Case\,1}$	12.195	1041.7	2.4268	491.28	34.834	-208.92	-3.5914	353.85	38025
$EL1_{Case\,2}$	12.195	917.08	7.6599	0.3808	32.350	-426.20	53.745	144.06	38025

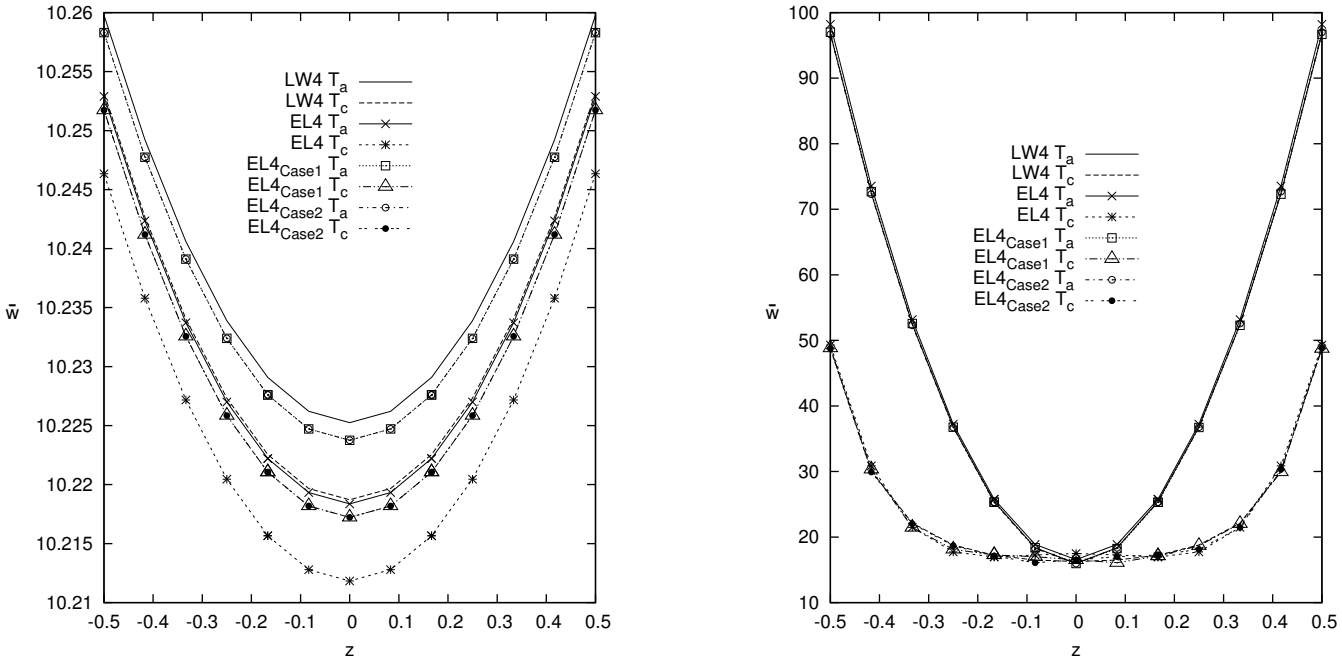

(a) (b)

Figure 9: Three-layered plate, transverse mechanical displacement $\hat{w}$, $a/h = 100$ (a), $a/h = 2$ (b).

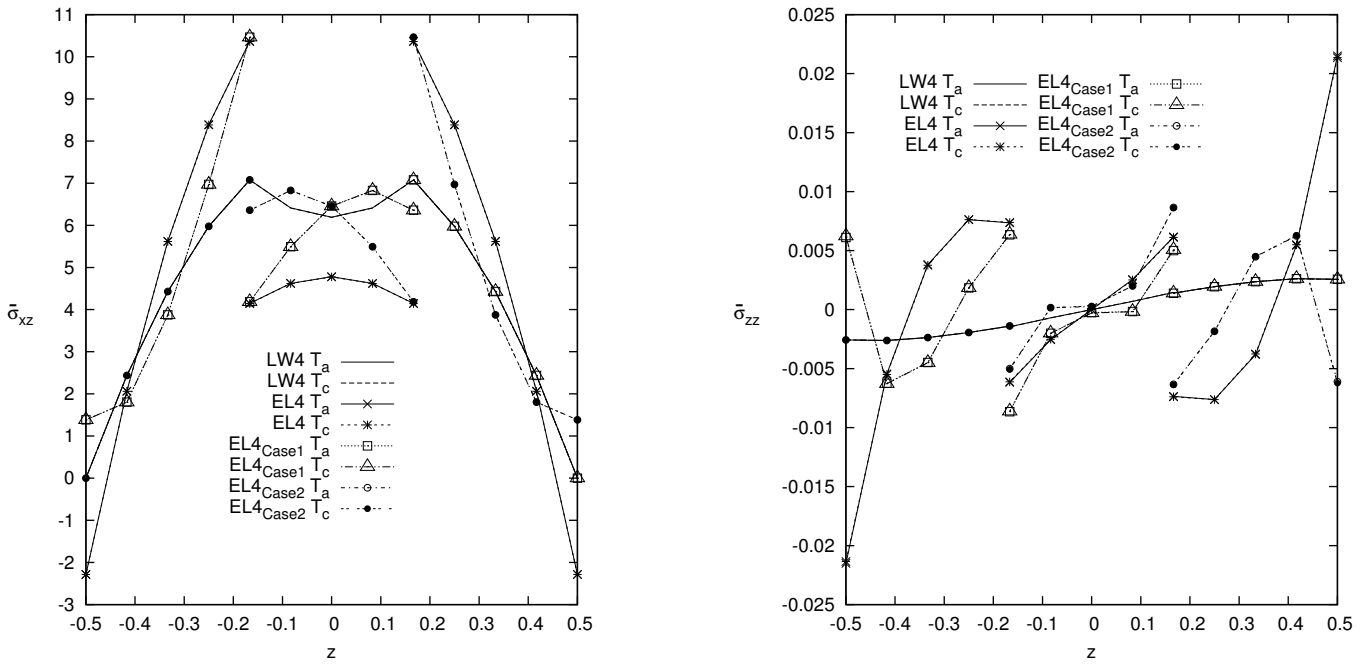

(a) (b)

Figure 10: Three-layered thin plates $a/h = 100$, transverse shear and normal stresses, $\hat{\sigma}_{xz}$ (a), $\hat{\sigma}_{zz}$ (b).

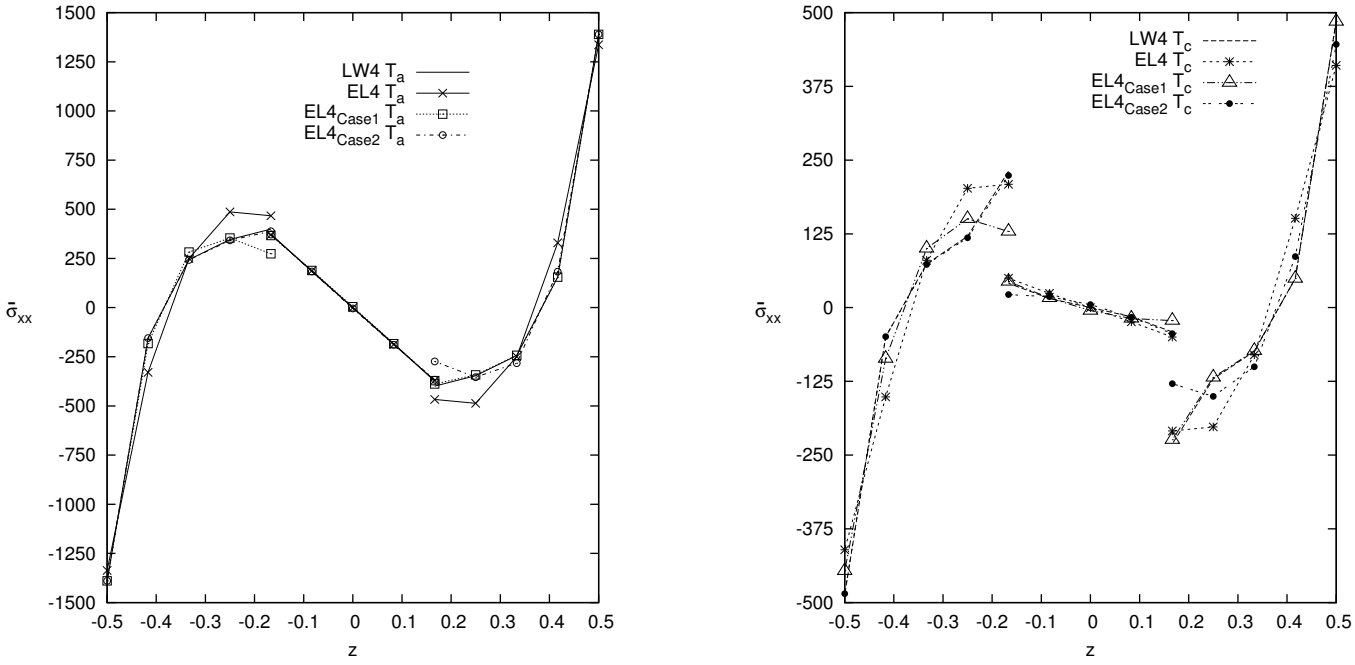

(a) (b)

Figure 11: Three-layered thick plates $a/h = 2$, in-plane stress $\hat{\sigma}_{xx}$, T_a assumed linear (a), T_c calculated via Fourier heat law (b).

Ten-layer cylindrical panel

A ten-layer cross-ply cylindrical shell panel with cross-ply composite layers with lamination $[0°/90°]_5$ and simply-supported boundary condition is considered. The Carbon-Epoxy material constants of the shell panel are taken from [7, 9], the values are expressed in terms of ratios of the longitudinal and transversal fiber directional properties : $\frac{E_1}{E_2} = 25,0$; $E_2 = E_3$; $\frac{G_{12}}{E_2} = 0,5$; $\frac{G_{23}}{E_2} = 0,2$; $G_{12} = G_{13}$; $\nu_{12} = \nu_{13} = \nu_{23} = 0,25$; $\frac{\alpha_2}{\alpha_1} = 3,0$; $\alpha_1 = \alpha_3$; $\frac{\mathcal{K}_1}{\mathcal{K}_2} = \frac{36,42}{0,96}$; $\mathcal{K}_2 = \mathcal{K}_3$. The geometrical dimensions are: $a = b = 1,0$ and $h_{total} = 0,1$. The temperature boundary conditions are: $\hat{\theta}_{top} = +0,5$, $\hat{\theta}_{bottom} = -0,5$. The results are presented for different radius to length side ratios $R/a = 5; 10; 50$, and the deflections and stresses are presented in the following dimensionless forms:

$$\hat{w} = \frac{w}{\alpha_1 \theta_1 b^2} \qquad \hat{\sigma}_{i,j} = \frac{\sigma_{i,j}}{E_2 \alpha_1 \theta_1}$$

where $\theta_1 = 1$. The adopted mesh is the same of the previous numerical example. Due to the symmetry of both the geometry and load, a quarter of the cylindrical shell panel is analyzed, see Figure 12, with a corresponding mesh grid of 16×16 elements. The corresponding thermal load, using the symmetry conditions, is defined as follows:

$$\theta(\alpha, \beta, z) = \hat{\theta}(z) \cos\left(\frac{m\pi\alpha}{a}\right) \cos\left(\frac{n\pi\beta}{b}\right) \tag{39}$$

where $m = n = 0, 5$. The symmetry condtions and the boundary conditions are defined as follows:

$$\begin{aligned}
u_\tau(\alpha, \beta) &= u_\tau(a/2, \beta) = 0 \\
v_\tau(\alpha, \beta) &= v_\tau(\alpha, b/2) = 0 \\
u_\tau(\alpha, \beta) &= u_\tau(\alpha, b) = 0 \\
v_\tau(\alpha, \beta) &= v_\tau(a, \beta) = 0 \\
w_\tau(\alpha, \beta) &= w_\tau(\alpha, b) = 0 \\
w_\tau(\alpha, \beta) &= w_\tau(a, \beta) = 0
\end{aligned} \tag{40}$$

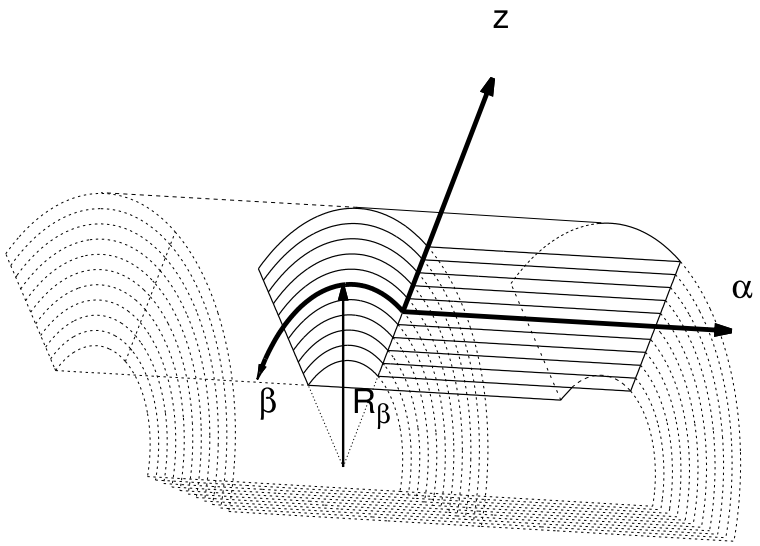

Figure 12: Reference system of the quarter of the composite cylindrical shell panel with symmetry condition applied.

The effect of the shell curvature on the temperature profile along the thickness of the multilayered cylindrical panel is given in Figure 13 for different radius to length ratios R/a. It has to be noticed that the curvature radius has no relevant influence on the approximation of the temperature load; as mentioned about the plate temperature profile discussion, the aspect ratio a/h shows the principal effect. It is preferable to use a calculated temperature profile to avoid to overestimate the temperature load.

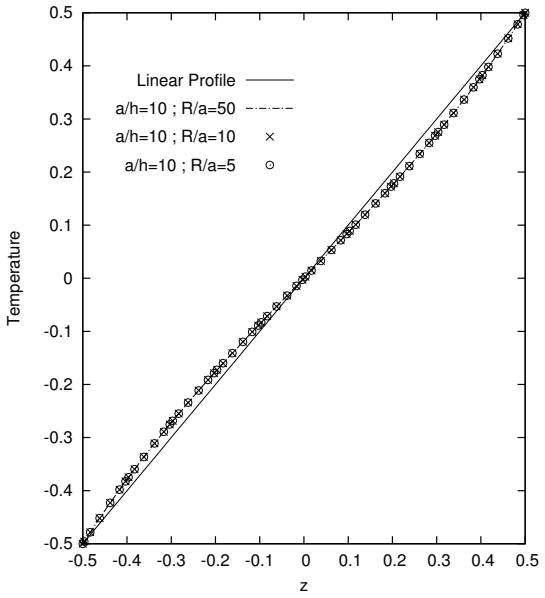

Figure 13: Ten-layered cylindrical shell panel. Temperature Profiles Comparison.

Different Variable Kinematic models, via the Legendre polynomials, have been used to perform the analysis of the shell structures. The acronyms have been modified adding a subscript to them, for the sake of clarity the list of subscripts is given below:

- $Case1 = \{layer1\}\,\{layer2, layer3, layer4, layer5, layer6, layer7, layer8, layer9\}\,\{layer10\}$
- $Case2 = \{layer1\}\,\{layer2\}\,\{layer3, layer4, layer5, layer6, layer7, layer8\}\,\{layer9\}\,\{layer10\}$
- $Case3 = \{layer1\}\,\{layer2\}\,\{layer3, layer4\}\,\{layer5, layer6\}\,\{layer7, layer8\}\,\{layer9\}\,\{layer10\}$
- $Case4 = \{layer1\}\,\{layer2, layer3\}\,\{layer4\}\,\{layer5, layer6\}\,\{layer7\}\,\{layer8, layer9\}\,\{layer10\}$

The results are listed in Table 4 for various radius to length side ratios R/a, and the degrees of freedom $DOFs$ are indicated for a quarter of the considered structure. The present FEs results are compared with an equivalent single layer model with cubic expansion in the z direction named $HOST12$ [7], and with an higher order shear deformation theory named $HSDT$ [9]. The transverse displacement $\hat{w}$ and the in-plane stress $\hat{\sigma}_{\alpha\alpha}$ show small accuracy differences for the considered cases R/a, see Table 4, this is due to the fixed aspect ratio $a/h = 10$. The difference of the variables magnitude is due to the different

description of the temperature profile, assumed linear profile for the upper part of the table results T_a and calculated solving the Fourier heat conduction equations for the lower part of the table results T_c. The behavior of the transverse shear stress $\hat{\sigma}_{\alpha z}$ along the thickness is not simple to well describe; for example for the assumed linear temperature profile T_a, the full equivalent-single-layer model $EL4$ is not able to perform the discontinuous nature of the shear stress along the thickness, see Figure 14a. The Variable-Kinematic model $EL4_{Case2}$ and $EL4_{Case3}$ show different level of accuracy respect to the full layer-wise solution $LW4$, meanwhile the model $EL4_{Case4}$ seems to describe well the shear stress along the thickness with small loss of accuracy in the layers with an ESL description and with a regardable $-29,27\%$ $DOFs$ reduction respect to the full layer-wise solution $LW4$, see Figure 14b.

As already mentioned for the shear stress, the description of the transverse normal stress $\hat{\sigma}_{zz}$ is not simple to perform too. For example, for the calculated temperature profile T_c, see Figure 15a, the full equivalent-single-layer $EL4$ model is not sufficient to correctly describe the stress profile along the thickness. Relevant improvements of the solution accuracy are shown by the Variable-Kinematic model $EL4_{Case2}$ and $EL4_{Case3}$. These Variable-Kinematic models permit to have noticeable reduction of the computational cost in terms of degrees of freedom; for example a $-29,27\%$ $DOFs$ reduction respect to the full layer-wise solution $LW4$ is obtained by the model $EL4_{Case4}$, see Figure 15b, with very small loss in the solution accuracy in the layers with an ESL description.

Table 4: Ten-layer composite cylindrical shell panel with lamination $[0°/90°]_5$. Mechanical variables described by Mono-models and Variable kinematic models for various radius to length side ratios R/a. Evaluation position for transverse displacement $\hat{w}(x,y,z) = \hat{w}(a/2, b/2, 0)$, in-plane stress $\hat{\sigma}_{\alpha\alpha}(x,y,z) = \hat{\sigma}_{\alpha\alpha}(a/2, b/2, +h/2)$, transverse shear stress $\hat{\sigma}_{\alpha z}(x,y,z) = 10 \times \hat{\sigma}_{\alpha z}(a, b/2, +\frac{2}{5}h)$, transverse normal stress $\hat{\sigma}_{zz}(x,y,z) = 10^2 \times \hat{\sigma}_{zz}(a/2, b/2, 0)$.

T_a (Assumed Linear)

	$R/a = 50$				$R/a = 5$				$DOFs$
	$\hat{w}$	$\hat{\sigma}_{\alpha\alpha}$	$\hat{\sigma}_{\alpha z}$	$\hat{\sigma}_{zz}$	$\hat{w}$	$\hat{\sigma}_{\alpha\alpha}$	$\hat{\sigma}_{\alpha z}$	$\hat{\sigma}_{zz}$	
$HOST12$[7]	1.0325	-	-	-	1.0224	-	-	-	
$HSDT$[9]	1.0332	-	-	-	1.0216	-	-	-	
$LW4$	1.0306	-0.9823	0.1368	0.0263	1.0207	-0.9789	0.1651	0.2817	133947
$LW1$	1.0306	-1.0023	0.0188	8.0403	1.0207	-0.9990	0.0448	8.3176	35937
$EL3Z$	1.0302	-0.9825	0.1123	0.0190	1.0205	-0.9792	0.1226	0.2852	16335
$EL4$	1.0301	-0.9827	0.1064	0.0038	1.0210	-0.9794	0.1383	0.2660	16335
$EL3$	1.0301	-0.9825	0.1079	0.0037	1.0210	-0.9792	0.1386	0.2660	13068
$EL2$	1.0271	-0.9851	-0.0207	-0.0037	1.0186	-0.9810	0.0275	0.1826	9801
$EL1$	1.0656	-1.1649	0.0016	0.0162	1.0575	-1.1611	0.0481	0.4828	6534
$EL4_{Case\,1}$	1.0303	-0.9825	0.0974	0.0033	1.0211	-0.9790	0.1116	0.2677	42471
$EL4_{Case\,2}$	1.0304	-0.9824	0.1369	0.0042	1.0211	-0.9789	0.1651	0.2669	68607
$EL4_{Case\,3}$	1.0306	-0.9823	0.1368	0.0042	1.0208	-0.9789	0.1651	0.2650	94743
$EL4_{Case\,4}$	1.0306	-0.9823	0.1500	0.0043	1.0208	-0.9789	0.1883	0.2651	94743
$EL1_{Case\,1}$	1.0499	-0.9934	0.0050	0.0108	1.0413	-0.9899	0.0577	0.4065	13068
$EL1_{Case\,2}$	1.0402	-0.9990	0.0075	0.0101	1.0311	-0.9956	0.0337	0.3525	19602
$EL1_{Case\,3}$	1.0314	-1.0023	0.0190	0.0048	1.0222	-0.9989	0.0451	0.2773	26136
$EL1_{Case\,4}$	1.0315	-1.0019	0.0111	0.0049	1.0222	-0.9985	0.0555	0.2766	26136

T_c (Calculated via Fourier Heat conduction Law)

	$R/a = 50$				$R/a = 5$				$DOFs$
	$\hat{w}$	$\hat{\sigma}_{\alpha\alpha}$	$\hat{\sigma}_{\alpha z}$	$\hat{\sigma}_{zz}$	$\hat{w}$	$\hat{\sigma}_{\alpha\alpha}$	$\hat{\sigma}_{\alpha z}$	$\hat{\sigma}_{zz}$	
$LW4$	0.9706	-1.0226	0.1443	0.0198	0.9613	-1.0194	0.1708	0.2155	133947
$LW1$	0.9707	-1.0498	0.0343	6.6928	0.9613	-1.0465	0.0588	6.9191	35937
$EL3Z$	0.9698	-1.0377	0.1231	0.6375	0.9606	-1.0344	0.1329	0.8491	16335
$EL4$	0.9699	-1.0231	0.1288	0.0141	0.9613	-1.0198	0.1587	0.2372	16335
$EL3$	0.9697	-1.0388	0.1198	0.0137	0.9611	-1.0355	0.1489	0.2223	13068
$EL2$	0.9654	-1.0428	-0.0702	0.0105	0.9573	-1.0388	-0.0246	0.1826	9801
$EL1$	1.0018	-1.2114	0.0015	0.0311	0.9941	-1.2078	0.0451	0.4673	6534
$EL4_{Case\,1}$	0.9698	-1.0228	0.1254	0.0130	0.9611	-1.0195	0.1386	0.2269	42471
$EL4_{Case\,2}$	0.9698	-1.0228	0.1444	0.0130	0.9610	-1.0195	0.1709	0.2197	68607
$EL4_{Case\,3}$	0.9705	-1.0226	0.1443	0.0112	0.9613	-1.0194	0.1709	0.2128	94743
$EL4_{Case\,4}$	0.9706	-1.0226	0.1582	0.0113	0.9613	-1.0194	0.1942	0.2130	94743
$EL1_{Case\,1}$	0.9869	-1.0420	-0.0098	0.0247	0.9787	-1.0386	0.0398	0.3828	13068
$EL1_{Case\,2}$	0.9780	-1.0471	0.0249	0.0212	0.9694	-1.0438	0.0494	0.3176	19602
$EL1_{Case\,3}$	0.9705	-1.0500	0.0349	0.0133	0.9618	-1.0467	0.0594	0.2287	26136
$EL1_{Case\,4}$	0.9712	-1.0494	0.0185	0.0145	0.9624	-1.0461	0.0603	0.2287	26136

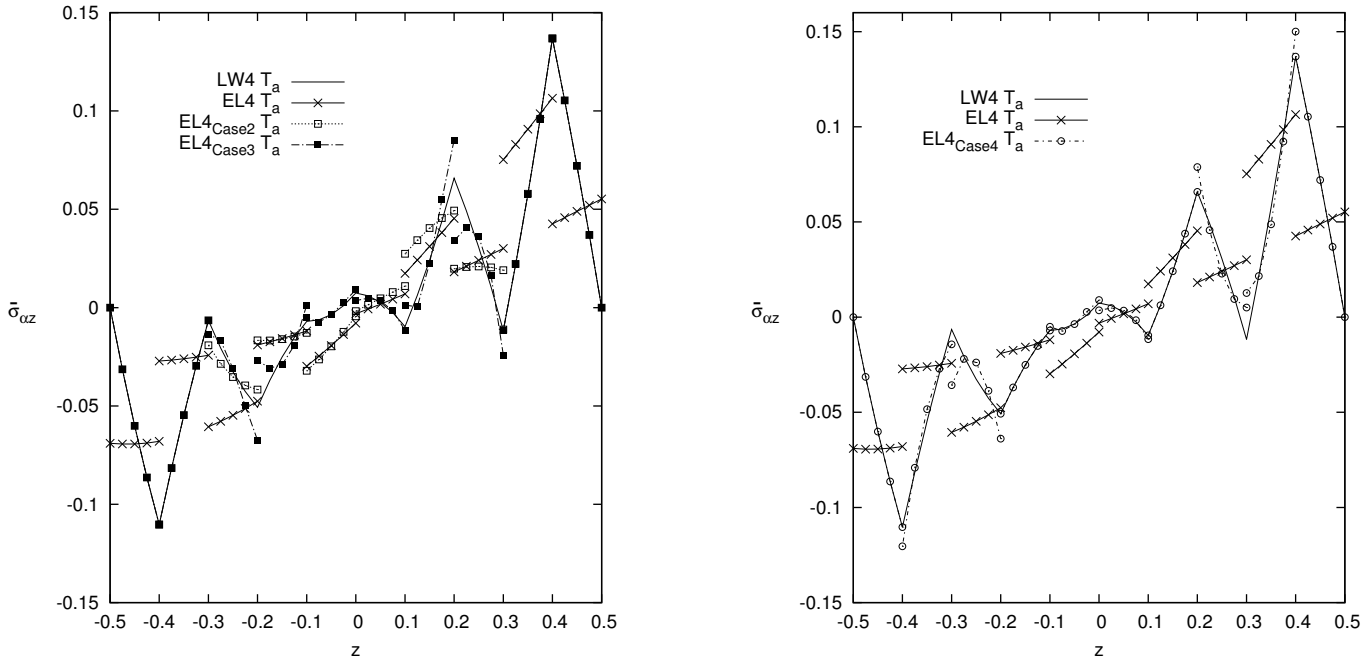

(a) (b)

Figure 14: Ten-layered cylindrical shell panel $R/a = 50$, transverse shear stress $\hat{\sigma}_{\alpha z}$, T_a assumed linear.

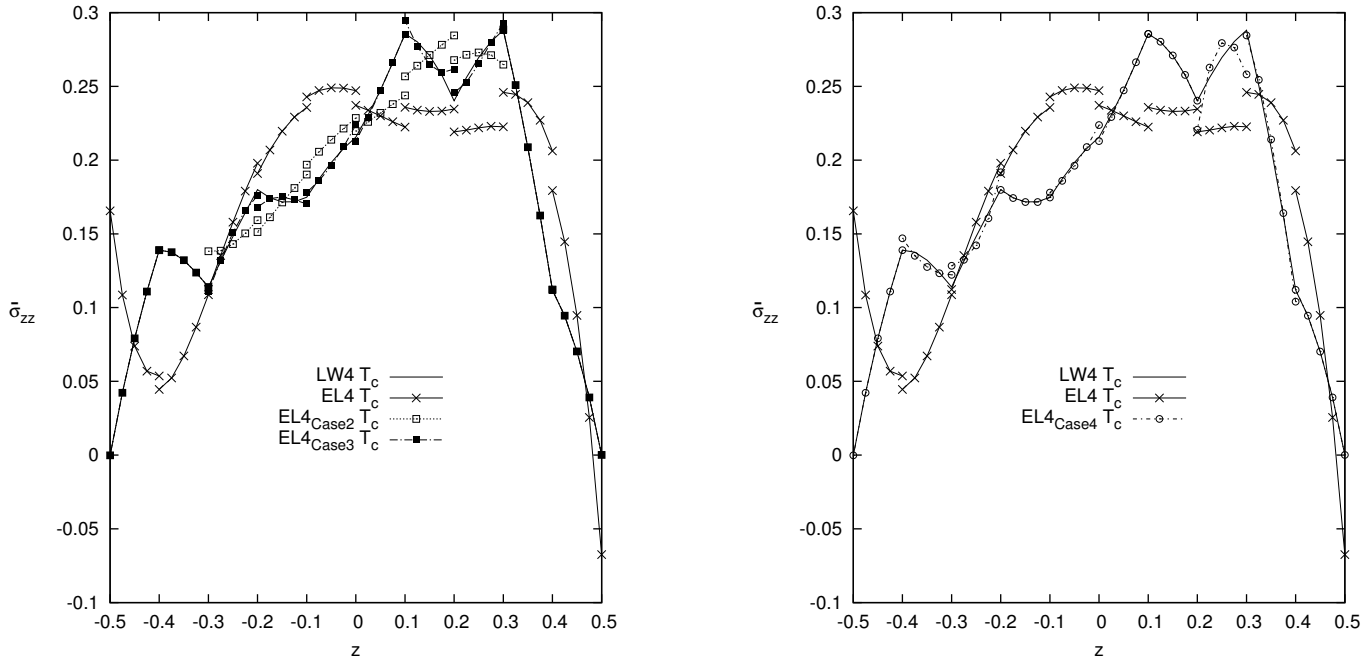

(a) (b)

Figure 15: Ten-layered cylindrical shell panel $R/a = 5$, transverse normal stress $\hat{\sigma}_{zz}$, T_c calculate via Fourier heat conduction law.

Sandwich composite spherical panel

A sandwich spherical shell panel with cross-ply composite skins with lamination $[0°/90°/Core/90°/0°]$ and simply-supported boundary condition is considered. The physical properties of the sandwich spherical panel are taken from [7, 30]. The material constants of the Carbon-Epoxy skins are: $E_1 = 172,37\,GPa$; $E_2 = E_3 = 6,89\,GPa$; $G_{12} = G_{13} = 3,45\,GPa$; $G_{23} = 1,38\,GPa$; $\nu_{12} = \nu_{13} = \nu_{23} = 0,25$; $\alpha_1 = \alpha_3 = 0,1 \times 10^{-5}\,\frac{1}{°C}$; $\alpha_2 = 2,0 \times 10^{-5}\,\frac{1}{°C}$; $\mathcal{K}_1 = 36,42\,W/(m\,°C)$; $\mathcal{K}_2 = \mathcal{K}_3 = 0,96\,W/(m\,°C)$. The material properties of the Honeycomb soft core are: $E_1 = E_2 = 0,28\,GPa$; $E_3 = 3,45\,GPa$; $G_{12} = 0,11\,GPa$; $G_{13} = G_{23} = 0,41\,GPa$; $\nu_{12} = \nu_{13} = \nu_{23} = 0,02$; $\alpha_1 = \alpha_3 = 0,1 \times 10^{-6}\,\frac{1}{°C}$; $\alpha_2 = 2,0 \times 10^{-6}\,\frac{1}{°C}$; $\mathcal{K}_1 = 3,642\,W/(m\,°C)$; $\mathcal{K}_2 = \mathcal{K}_3 = 0,096\,W/(m\,°C)$. The geometrical dimensions are: $a = b = 1,0$; the core thickness is $h_{core} = 0,8 \times h_{total}$ and each skin is $h_{skin} = 0,05 \times h_{total}$.

The temperature boundary conditions are: $\hat{\theta}_{top} = +0,5$, $\hat{\theta}_{bottom} = -0,5$. The results are presented for different radius to length side ratios $R/a = 5;20$ and different aspect ratios $a/h = 4;100$, and the deflections and stresses are presented in the following dimensionless forms:

$$\hat{w} = \frac{w}{\alpha_1 \theta_1 b^2} \qquad \hat{\sigma}_{i,j} = \frac{\sigma_{i,j}}{E_2 \alpha_1 \theta_1}$$

where $\theta_1 = 1$, E_2 and α_1 are the properties of the composite skins. The adopted mesh is the same of the previous numerical example. Due to the symmetry of both the geometry and load, a quarter of the spherical shell panel is analyzed, see Figure 16, with a corresponding mesh grid of 16×16 elements. The corresponding thermal load and boundary conditions are the same of previous numerical example.

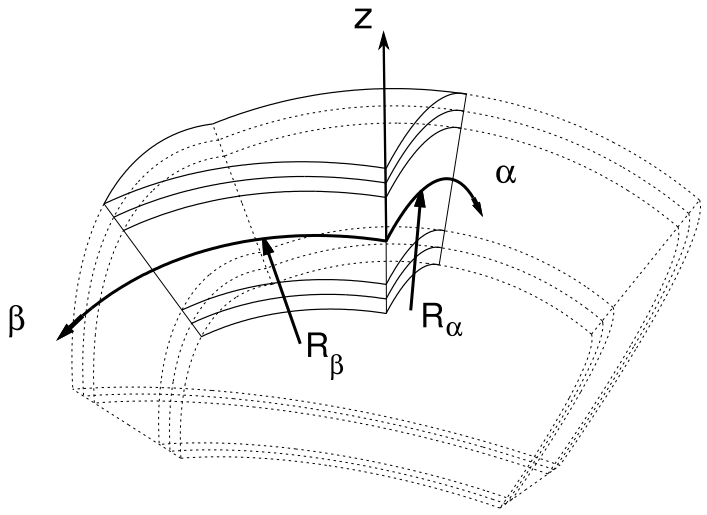

Figure 16: Reference system of the quarter of the sandwich spherical shell panel with symmetry condition applied.

The description of the temperature profile along the thickness of the sandwich spherical panel is discussed for different radius to length ratios R/a and aspect ratios a/h. It has to be noticed that for thin shells, see Figure 17a, the calculated temperature profile is far from the linear one, and differently from the previous numerical example the linear profile is underestimating the temperature load. For thick shells, see Figure 17b, the calculated profile has a non-linear behavior along the thickness direction,

the linear profile is both underestimating and overestimating the temperature load in different part of the multilayered structure. Looking at the results of the thick sandwich spherical shells, the global effect is that the linear profile is underestimating the temperature load. For both the thin and thick shells the radius to length ratios R/a is not showing any relevant effect on the calculated temperature profiles.

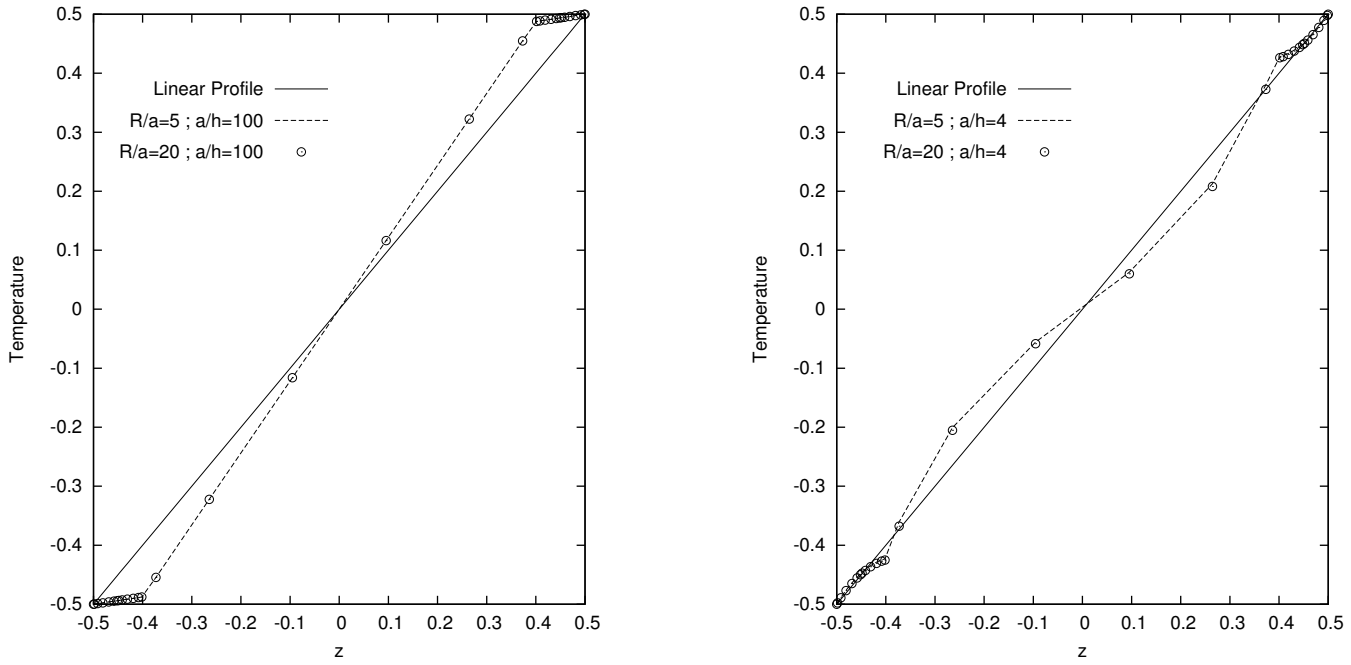

(a) (b)

Figure 17: Five-layered sandwich spherical shell panel. Temperature Profiles Comparison. $a/h = 100$ (a), $a/h = 4$ (b)

Different Variable Kinematic models, via the Legendre polynomials, have been used to perform the analysis of the shell structures. The acronyms have been modified adding a subscript to them, for the sake of clarity the list of subscripts is given below:

- $Case1 = \{layer1\}\,\{layer2, layer3, layer4\}\,\{layer5\}$
- $Case2 = \{layer1, layer2\}\,\{layer3, layer4, layer5\}$

- $Case3 = \{layer1, layer2\}\,\{layer3\}\,\{layer4, layer5\}$

The results are listed in Table 5 with a temperature profile assumed linear T_a for various radius to length side ratios R/a and various aspect ratios a/h, and the degrees of freedom $DOFs$ are indicated for a quarter of the considered structure. The present FEs results are compared with an equivalent single layer model with cubic expansion in the z direction named $HOST12$ [7], and with two analytical models, a layer-wise theory of the fourth order named $LW4_a$ [30] and an equivalent-single-layer theory of the fourth order with Taylor polynomials named $ET4_a$ [30]. Therefore the temperature profile calculated solving the Fourier heat conduction equations T_c is evaluated and the results are presented in Table 6 for various radius to length side ratios R/a and various aspect ratios a/h. The following considerations can be drawn:

- Regarding the transverse displacement w, for thin plates $a/h = 100$, the theories $EL4_{,Case1}$ and $EL4_{,Case2}$ lead an improvement of the solution respect to the $EL4$, and the model $EL4_{,Case3}$ show the same accuracy of the full layer-wise solution $LW4$ with a reduction of $-38,1\,\%$ $DOFs$ respect the $LW4$ theory, see Figure 18a. The same comments can be drawn for both the temperature assumed linear cases T_a and for the temperature calculated via the Fourier heat conduction law T_c. For thick plates $a/h = 2$, the description of the transverse displacement is well drawn only by $EL4_{,Case3}$ that show an accuracy very close to the full layer-wise solution $LW4$, see Figure 18b.

- For the in-plane stress $\sigma_{\alpha\alpha}$ no relevant differences can be appreciated between all the presented models.

- Regarding the transverse shear stress $\sigma_{\alpha z}$, the variable kinematic model $EL4_{,Case1}$ improves the results respect to the $EL4$ theory only in the layer with a layer-wise description, see Figure 19a. The theories $EL4_{,Case3}$ can improve the results along the whole thickness with some errors in the description of the composite skins, see Figure 19b.

- For the transverse normal stress σ_{zz}, the variable kinematic model $EL4_{,Case1}$ improves the results respect to the $EL4$ theory only in the layer with a layer-wise description, see Figure 20a. The theories $EL4_{,Case3}$ has the same accuracy of the full layer-wise solution along the whole thickness of the spherical sandwich panel, see Figure 20b.

Table 5: Five-layer sandwich spherical shell panel with lamination $[0°/90°/Core/90°/0°]$. Mechanical variables described by Mono-models and Variable kinematic models for various radius to length side ratios R/a and various aspect ratios a/h. Evaluation position for transverse displacement $\hat{w}(x,y,z) = \hat{w}(a/2,b/2,0)$, in-plane stress $\hat{\sigma}_{\alpha\alpha}(x,y,z) = \hat{\sigma}_{\alpha\alpha}(a/2,b/2,+h/2)$, transverse shear stress $\hat{\sigma}_{\alpha z}(x,y,z) = 10 \times \hat{\sigma}_{\alpha z}(a,b/2,+\frac{9}{20}h)$, transverse normal stress $\hat{\sigma}_{zz}(x,y,z) = 10^2 \times \hat{\sigma}_{zz}(a/2,b/2,0)$. The temperature profile is assumed linear T_a.

$a/h = 100$

	$R/a=20$				$R/a=5$				$DOFs$
	$\hat{w}$	$\hat{\sigma}_{\alpha\alpha}$	$\hat{\sigma}_{\alpha z}$	$\hat{\sigma}_{zz}$	$\hat{w}$	$\hat{\sigma}_{\alpha\alpha}$	$\hat{\sigma}_{\alpha z}$	$\hat{\sigma}_{zz}$	
$HOST12$[7]	1.6614	-	-	-	0.7332	-	-	-	
$LW4$	1.6296	6.9442	-0.1049	0.0165	0.7178	-3.1483	0.0603	0.2818	68607
$LW1$	1.6298	6.9005	-0.0431	0.0172	0.7179	-3.1968	0.0419	0.2837	19602
$EL3Z$	1.6619	7.0796	-0.0209	0.3365	0.7333	-3.2259	0.2987	0.8667	16335
$EL4$	1.6387	7.2355	-0.0405	0.3199	0.7223	-2.8967	0.3029	0.8617	16335
$EL3$	1.6620	7.0788	-0.0424	0.3135	0.7334	-3.2272	0.3057	0.8269	13068
$EL2$	1.6623	7.0792	-0.0015	-0.5764	0.7349	-3.2468	0.7680	-0.8356	9801
$EL1$	1.7362	7.4627	0.0282	-0.5819	0.7711	-3.3300	0.8482	-0.7890	6534
$EL4_{Case\,1}$	1.6378	7.0512	-0.1065	0.2951	0.7219	-3.0907	0.0596	0.8051	42471
$EL4_{Case\,2}$	1.6345	6.9486	-0.1335	6.8462	0.7195	-3.1891	0.1277	7.7908	29403
$EL4_{Case\,3}$	1.6296	6.9443	-0.1335	0.0165	0.7178	-3.1483	0.1265	0.2819	42471
$EL1_{Case\,1}$	1.6775	7.5348	-0.0480	-0.3343	0.7418	-2.8316	0.0394	-0.3409	13068
$EL1_{Case\,2}$	1.6696	6.9080	-0.0639	-26.156	0.7337	-3.5591	0.1289	-28.658	9801
$EL1_{Case\,3}$	1.6301	6.8592	-0.0639	0.0172	0.7181	-3.2449	0.1224	0.2837	13068

$a/h = 4$

	$R/a=20$				$R/a=5$				$DOFs$
	$\hat{w}$	$\hat{\sigma}_{\alpha\alpha}$	$\hat{\sigma}_{\alpha z}$	$\hat{\sigma}_{zz}$	$\hat{w}$	$\hat{\sigma}_{\alpha\alpha}$	$\hat{\sigma}_{\alpha z}$	$\hat{\sigma}_{zz}$	
$HOST12$[7]	1.7959	-	-	-	1.7738	-	-	-	
$LW4_a$[30]	1.8259	-	-	-	1.8059	-	-	-	
$ET4_a$[30]	1.8370	-	-	-	1.8125	-	-	-	
$LW4$	1.8254	6.5416	-2.7197	0.1938	1.8052	6.6884	-2.6941	0.7940	68607
$LW1$	1.8241	6.4558	-1.1339	0.2070	1.8038	6.6040	-1.1245	0.8482	19602
$EL3Z$	1.7897	6.6392	-1.0356	-0.0284	1.7700	6.7748	-1.0097	-0.0901	16335
$EL4$	1.8371	6.7068	-1.5927	0.2405	1.8184	6.8654	-1.5633	0.9855	16335
$EL3$	1.7954	6.6231	-1.6543	-0.0264	1.7759	6.7600	-1.6257	-0.0820	13068
$EL2$	1.6641	6.2299	-1.1041	0.1285	1.6548	6.3836	-1.0617	0.5291	9801
$EL1$	1.9033	6.5229	-0.7331	0.5996	1.8922	6.6269	-0.7111	2.4134	6534
$EL4_{Case\,1}$	1.8503	6.6151	-2.7443	0.2290	1.8314	6.7656	-2.7192	0.9378	42471
$EL4_{Case\,2}$	1.8408	6.5387	-3.5575	6.8849	1.8224	6.6884	-3.5236	7.6024	29403
$EL4_{Case\,3}$	1.8236	6.5457	-3.5647	0.1936	1.8034	6.6922	-3.5297	0.7932	42471
$EL1_{Case\,1}$	1.8601	6.7508	-1.2004	0.4221	1.8458	6.9087	-1.1911	1.7059	13068
$EL1_{Case\,2}$	1.7971	6.0653	-1.7360	-24.504	1.7960	6.2311	-1.7219	-23.352	9801
$EL1_{Case\,3}$	1.8109	6.3652	-1.8325	0.2061	1.7910	6.5116	-1.8116	0.8445	13068

Table 6: Five-layer sandwich spherical shell panel with lamination $[0°/90°/Core/90°/0°]$. Mechanical variables described by Mono-models and Variable kinematic models for various radius to length side ratios R/a and various aspect ratios a/h. Evaluation position for transverse displacement $\hat{w}(x,y,z) = \hat{w}(a/2,b/2,0)$, in-plane stress $\hat{\sigma}_{\alpha\alpha}(x,y,z) = \hat{\sigma}_{\alpha\alpha}(a/2,b/2,+h/2)$, transverse shear stress $\hat{\sigma}_{\alpha z}(x,y,z) = 10 \times \hat{\sigma}_{\alpha z}(a,b/2,+\frac{9}{20}h)$, transverse normal stress $\hat{\sigma}_{zz}(x,y,z) = 10^2 \times \hat{\sigma}_{zz}(a/2,b/2,0)$. The temperature profile is calculated via Fourier heat conduction equation T_c.

$a/h = 100$									
	$R/a = 20$				$R/a = 5$				$DOFs$
	$\hat{w}$	$\hat{\sigma}_{\alpha\alpha}$	$\hat{\sigma}_{\alpha z}$	$\hat{\sigma}_{zz}$	$\hat{w}$	$\hat{\sigma}_{\alpha\alpha}$	$\hat{\sigma}_{\alpha z}$	$\hat{\sigma}_{zz}$	
$LW4$	1.7822	9.0011	-0.1253	0.0185	0.7850	-2.0364	0.0553	0.3101	68607
$LW1$	1.7823	9.0037	-0.0550	0.0193	0.7850	-2.0383	0.0379	0.3123	19602
$EL3Z$	1.8174	9.2487	-0.0317	0.3689	0.8019	-2.0210	0.3178	0.9518	16335
$EL4$	1.7932	9.4104	-0.0564	0.3509	0.7905	-1.6778	0.3194	0.9461	16335
$EL3$	1.8174	9.2478	-0.0584	0.3442	0.8020	-2.0224	0.3223	0.9098	13068
$EL2$	1.8178	9.2492	-0.0167	-0.6303	0.8036	-2.0431	0.8248	-0.9137	9801
$EL1$	1.8987	9.6691	0.0158	-0.6364	0.8433	-2.1342	0.9125	-0.8628	6534
$EL4_{Case\,1}$	1.7919	9.1278	-0.1272	0.3235	0.7898	-1.9682	0.0544	0.8835	42471
$EL4_{Case\,2}$	1.7879	9.0075	-0.1632	7.3768	0.7870	-2.0835	0.1225	8.4112	29403
$EL4_{Case\,3}$	1.7822	9.0011	-0.1633	0.0185	0.7850	-2.0364	0.1211	0.3101	42471
$EL1_{Case\,1}$	1.8379	9.7435	-0.0607	-0.3653	0.8128	-1.6140	0.0350	-0.3695	13068
$EL1_{Case\,2}$	1.8256	9.0597	-0.0814	-28.720	0.8023	-2.3859	0.1295	-31.455	9801
$EL1_{Case\,3}$	1.7822	9.0053	-0.0813	0.0193	0.7851	-2.0416	0.1224	0.3123	13068
$a/h = 4$									
	$R/a = 20$				$R/a = 5$				$DOFs$
	$\hat{w}$	$\hat{\sigma}_{\alpha\alpha}$	$\hat{\sigma}_{\alpha z}$	$\hat{\sigma}_{zz}$	$\hat{w}$	$\hat{\sigma}_{\alpha\alpha}$	$\hat{\sigma}_{\alpha z}$	$\hat{\sigma}_{zz}$	
$LW4$	1.8301	6.6442	-2.7929	0.1954	1.8102	6.8325	-2.7774	0.7999	68607
$LW1$	1.8278	6.5515	-1.1718	0.2127	1.8078	6.7420	-1.1679	0.8704	19602
$EL3Z$	1.7951	6.7499	-1.0524	-0.0426	1.7756	6.9282	-1.0335	-0.1473	16335
$EL4$	1.8426	6.8165	-1.6421	0.2351	1.8242	7.0193	-1.6195	0.9630	16335
$EL3$	1.8010	6.7329	-1.7036	-0.0317	1.7817	6.9141	-1.6818	-0.1037	13068
$EL2$	1.6760	6.3515	-1.1377	0.1692	1.6667	6.5495	-1.1031	0.6915	9801
$EL1$	1.9164	6.6461	-0.7640	0.6424	1.9053	6.7943	-0.7475	2.5840	6534
$EL4_{Case\,1}$	1.8572	6.7241	-2.8195	0.2096	1.8385	6.9166	-2.8046	0.8598	42471
$EL4_{Case\,2}$	1.8457	6.6422	-3.6752	6.8694	1.8276	6.8335	-3.6549	7.5752	29403
$EL4_{Case\,3}$	1.8282	6.6485	-3.6822	0.1952	1.8083	6.8365	-3.6608	0.7991	42471
$EL1_{Case\,1}$	1.8723	6.8700	-1.2427	0.4647	1.8580	7.0716	-1.2390	1.8761	13068
$EL1_{Case\,2}$	1.8064	6.1758	-1.8030	-24.714	1.8053	6.3862	-1.7970	-23.479	9801
$EL1_{Case\,3}$	1.8135	6.4685	-1.8977	0.2119	1.7940	6.6587	-1.8846	0.8669	13068

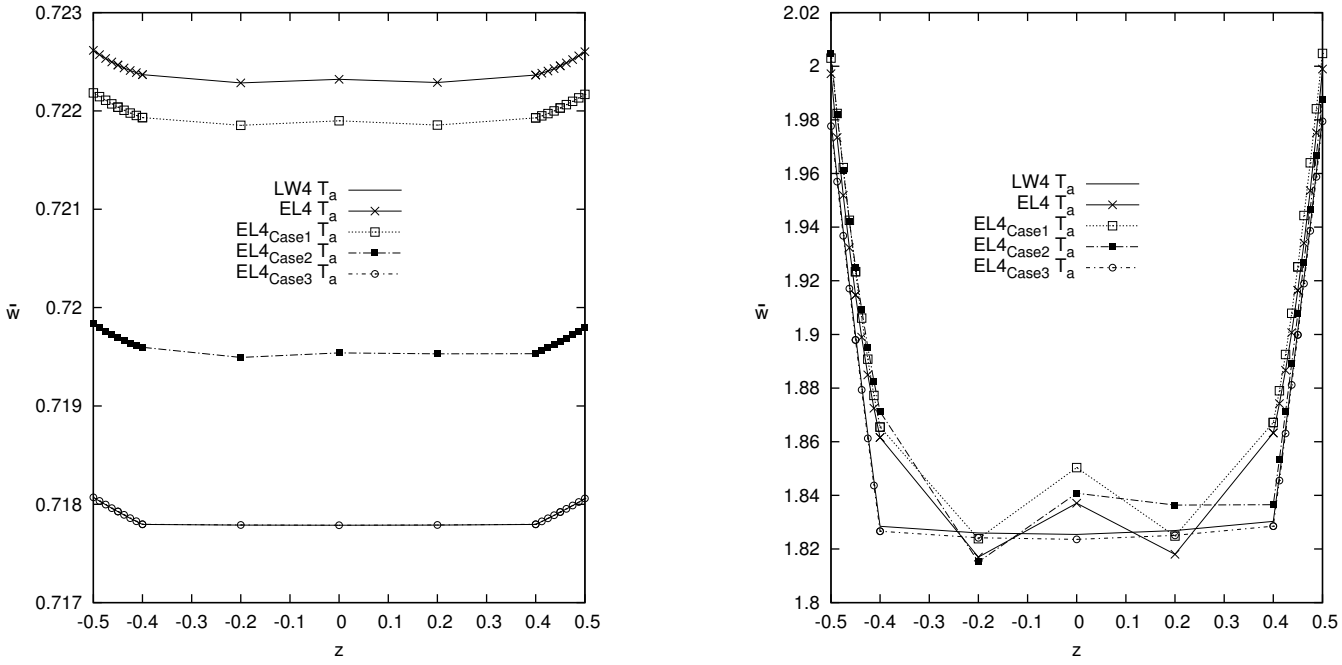

(a) (b)

Figure 18: Five-layered sandwich spherical panel transverse displacement $\hat{w}$ with an assumed linear temperature profile T_a, $R/a = 5$ and $a/h = 100$ (a), $R/a = 20$ and $a/h = 4$ (b)

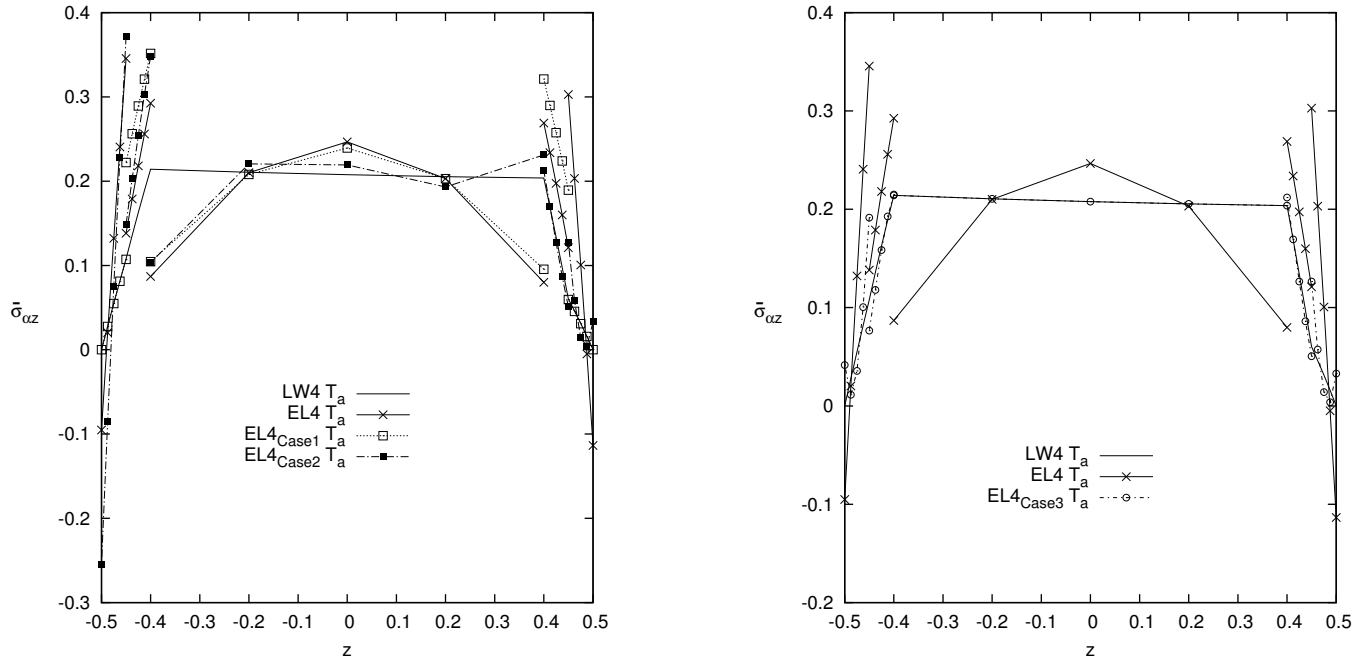

(a) (b)

Figure 19: Five-layered sandwich spherical panel transverse shear stress $\hat{\sigma}_{\alpha z}$ with an assumed linear temperature profile T_a, $R/a = 5$ and $a/h = 100$.

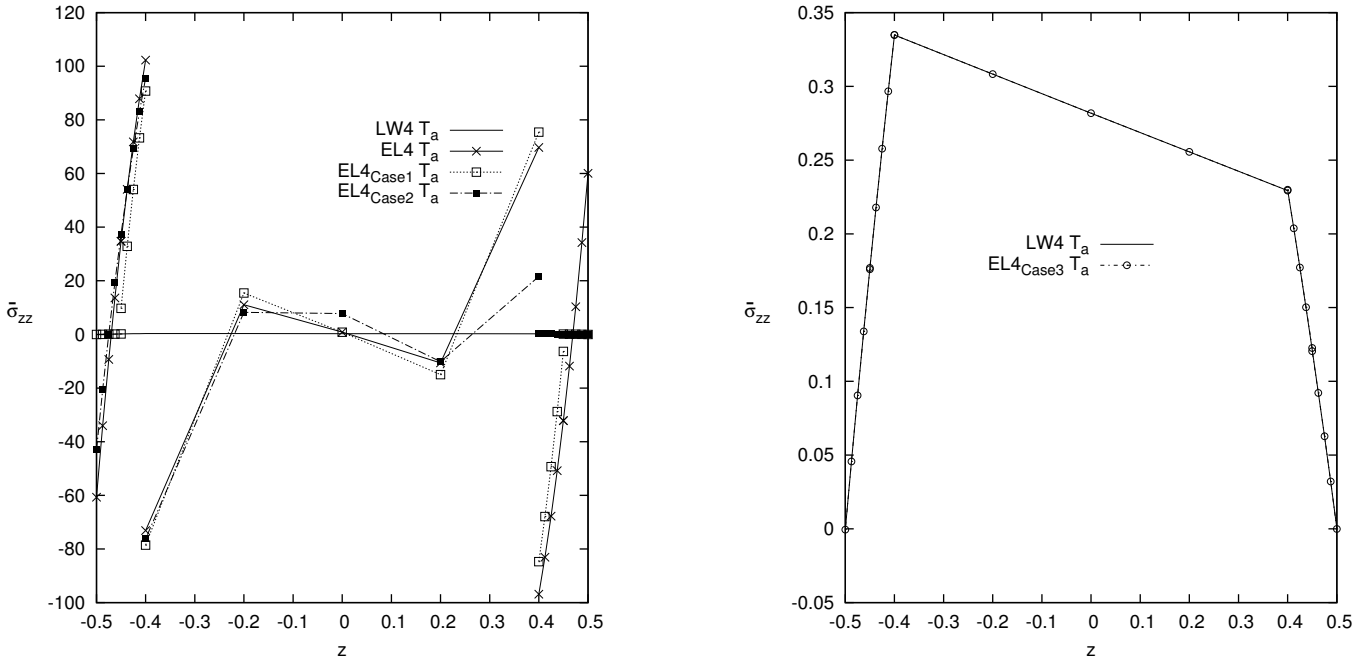

(a) (b)

Figure 20: Five-layered sandwich spherical panel transverse normal stress $\hat{\sigma}_{zz}$ with an assumed linear temperature profile T_a, $R/a = 5$ and $a/h = 100$.

Conclusions

This paper has dealt with the thermo-elastic static analysis of composite plates and shells using a two-dimensional finite element based on the Unified Formulation. The element has been assessed by analyzing cross-ply plates and multilayered composite cylindrical and sandwich spherical shells with simply-supported boundary conditions under bi-sinusoidal thermal loads. The results have been presented in terms of both transverse displacement, in-plane stresses, transverse shear stresses and transverse normal stress for various thickness ratios and radius to thickness ratios. The performances of the shell element have been tested, and the different theories (classical, refined, and Variable-Kinematic models) within the CUF framework have been compared. It is possible to conclude that the shell element with the MITC technique is locking free, for all the considered cases and for all the chosen models.

The results converge to the reference solution by increasing the order of expansion of the displacements in the thickness direction. For multilayered composite plates and shells, Variable-Kinematic models permit to improve the results with a reduction of computational costs, with respect to a full Layer-Wise solutions.Therefore the shear stresses can be modelized, in specific layers, by Variable-Kinematic models with the same accuracy of Layer-Wise theories, whereas strong reduction of computational costs can be obtained in the other layers. The sandwich core has to be modeled by a layer-wise description. The Variable-Kinematic model permits to improve globally the results, and at the same time permit to reduce the computational cost of the analysis, assembling the composite skins with an equivalent-single-layer model. In future works, the loss of accuracy of the behavior of the transverse shear and normal stresses can be solved adopting the RMVT principle in the layers with an equivalent-single-layer description.

References

[1] J. N. Reddy and D. H. Robbins, "Theories and computational models for composite laminates," *Appl. Mech. Rev.*, vol. 47, pp. 147–165, 1994.

[2] T. K. Varadan and K. Bhaskar, "Review of different theories for the analysis of composites," *Journal of Aerospace Society of India*, vol. 49, pp. 202–208, 1997.

[3] E. Carrera, "Developments, ideas and evaluation based upon Reissner's Mixed Variational Theorem in the Modeling of Multilayered Plates and Shells," *Appl. Mech. Rev.*, vol. 54, pp. 301–329, 2001.

[4] T. Kant and R. K. Khare, "Finite element thermal stress analysis of composite laminates using a higher-order theory," *J. Therm. Stresses*, vol. 17, no. 2, pp. 229–255, 1994.

[5] A. A. Khdeir and J. N. Reddy, "Thermal stresses and deflections of cross-ply laminated plates using refined plate theories," *J. Therm. Stresses*, vol. 14, no. 4, pp. 419–438, 1991.

[6] W. Zhen and C. Wanji, "A global-local higher order theory for multilayered shells and the analysis of laminated cylindrical shell panels," *Compos. Struct.*, vol. 84, no. 4, pp. 350–361, 2008.

[7] K. R. Khare, T. Kant, and A. K. Garg, "Closed-form thermo-mechanical solutions of higher-order theories of cross-ply laminated shallow shells," *Compos. Struct.*, vol. 59, pp. 313–340, 2003.

[8] A. A. Khdeir, "Thermoelastic analysis of cross-ply laminated circular cylindrical shells," *Int. J. Solids Struct.*, vol. 33, no. 27, pp. 4007–4017, 1996.

[9] A. A. Khdeir, M. B. Rajab, and J. N. Reddy, "Thermal effects on the response of cross-ply laminated shallow shells," *Int. J. Solids Struct.*, vol. 29, no. 5, pp. 653–667, 1992.

[10] A. Barut, E. Madenci, and A. Tessler, "Nonlinear thermoelastic analysis of composite panels under non-uniform temperature distribution," *Int. J. Solids Struct.*, vol. 37, no. 27, pp. 3681–3713, 2000.

[11] C. J. Miller, W. A. Millavec, and T. P. Richer, "Thermal stress analysis of layered cylindrical shells," *A.I.A.A. J.*, vol. 19, no. 4, pp. 523–530, 1981.

[12] P. C. Dumir, J. K. Nath, P. Kumari, and S. Kapuria, "Improved efficient zigzag and third order theories for circular cylindrical shells under thermal loading," *J. Therm. Stresses*, vol. 31, no. 4, pp. 343–367, 2008.

[13] Y. S. Hsu, J. N. Reddy, and C. W. Bert, "Thermoelasticity of circular cylindrical shells laminated of bimodulus composite materials.," *J. Therm. Stresses*, vol. 4, no. 2, pp. 155–177, 1981.

[14] K. Ding, "Thermal stresses of weak formulation study for thick open laminated shell," *J. Therm. Stresses*, vol. 31, no. 4, pp. 389–400, 2008.

[15] A. S. D. Wang and F. W. Crossman, "Calculation of Edge Stresses in Multi-Layer by Sub-Structuring," *J. Compos. Mater.*, vol. 12, pp. 76–83, 1978.

[16] N. J. Pagano and S. R. Soni, "Global-Local Laminate Variational Model," *Int. J. Solids Struct.*, vol. 19, no. 3, pp. 207–228, 1983.

[17] R. Jones, R. Callinan, K. K. Teh, and K. C. Brown, "Analysis of Multi-Layer Laminates Using Three-Dimensional Super Elements," *Int. J. Numer. Meth. Eng.*, vol. 20, no. 3, pp. 583–587, 1984.

[18] A. Pagani, S. Valvano, and E. Carrera, "Analysis of laminated composites and sandwich structures by variable-kinematic MITC9 plate elements," *J. Sandw. Struct. Mater.*

[19] S. Valvano, A. Pagani, and E. Carrera, "Analysis of Laminated Composites and Sandwich Structures by Variable-Kinematic Shell Elements," *Submitted*.

[20] M. Botshekanan Dehkordi, M. Cinefra, S. M. R. Khalili, and E. Carrera, "Mixed LW/ESL models for the analysis of sandwich plates with composite faces," *Compos. Struct.*, vol. 98, pp. 330–339, 2013.

[21] M. Botshekanan Dehkordi, S. M. R. Khalili, and E. Carrera, "Non-linear transient dynamic analysis of sandwich plate with composite face-sheets embedded with shape memory alloy wires and flexible core- Based on the mixed LW (Layer-wise)/ESL (Equivalent single layer) models," *Compos. Part B-Eng.*, vol. 87, pp. 59–74, 2016.

[22] E. Carrera, "Theories and finite elements for multilayered, anisotropic, composite plates and shells," *Arch. Comput. Method. E*, vol. 9, no. 2, pp. 87–140, 2002.

[23] E. Carrera, "Theories and finite elements for multilayered plates and shells: a unified compact formulation with numerical assessment and benchmarking," *Arch. Comput. Method. E*, vol. 10, no. 3, pp. 215–296, 2003.

[24] E. Carrera, "Temperature profile influence on layered plates response considering classical and advanced theories," *A.I.A.A. J.*, vol. 40, no. 9, pp. 1885–1896, 2002.

[25] P. Nali, E. Carrera, and A. Calvi, "Advanced fully coupled thermo-mechanical plate elements for multilayered structures subjected to mechanical and thermal loading," *Int. J. Numer. Meth. Eng.*, vol. 85, pp. 869–919, 2011.

[26] E. Carrera and A. Ciuffreda, "Closed-form solutions to assess multilayered-plate theories for various thermal stress problems," *J. Therm. Stresses*, vol. 27, pp. 1001–1031, 2004.

[27] E. Carrera, "An assessment of mixed and classical theories for the thermal stress analysis of orthotropic multilayered plates," *J. Therm. Stresses*, vol. 23, no. 9, pp. 797–831, 2000.

[28] A. Robaldo and E. Carrera, "Mixed finite elements for thermoelastic analysis of multilayered anisotropic plates," *J. Therm. Stresses*, vol. 30, pp. 165–194, 2007.

[29] S. Brischetto, R. Leetsch, E. Carrera, T. Wallmersperger, and B. Kröplin, "Thermo-mechanical bending of functionally graded plates," *J. Therm. Stresses*, vol. 31, no. 3, pp. 286–308, 2008.

[30] S. Brischetto and E. Carrera, "Thermal Stress Analysis by Refined Multilayered Composite Shell Theories," *J. Therm. Stresses*, vol. 32, pp. 165–186, 2009.

[31] S. Brischetto and E. Carrera, "Heat conduction and thermal analysis in multilayered plates and shells," *Mech. Res. Commun.*, vol. 38, pp. 449–455, 2011.

[32] M. Cinefra, E. Carrera, S. Brischetto, and S. Belouettar, "Thermo-mechanical analysis of functionally graded shells," *J. Therm. Stresses*, vol. 33, pp. 942–963, 2010.

[33] K. J. Bathe and E. Dvorkin, "A formulation of general shell elements - the use of mixed interpolation of tensorial components," *Int. J. Numer. Meth. Eng.*, vol. 22, pp. 697–722, 1986.

[34] K. J. Bathe and F. Brezzi, "A simplified analysis of two plate bending elements-the MITC4 and MITC9 elements," *Proc. Numerical Methods in Engineering: Theory and Applications*, 1987.

[35] K. J. Bathe, P. S. Lee, and J. F. Hiller, "Towards improving the MITC9 shell element," *Comput. Struct.*, vol. 81, pp. 477–489, 2003.

[36] N. C. Huang, "Membrane locking and assumed strain shell elements," *Comput. Struct.*, vol. 27, no. 5, pp. 671–677, 1987.

[37] M. Cinefra, S. Valvano, and E. Carrera, "Heat conduction and Thermal Stress Analysis of laminated composites by a variable kinematic MITC9 shell element," *Curved and Layered Structures*, vol. 1, pp. 301–320, 2015.

[38] M. Cinefra, E. Carrera, and S. Valvano, "Variable Kinematic Shell Elements for the Analysis of Electro-Mechanical Problems," *Mech. Adv. Mater. Struc.*, vol. 22, no. 1-2, pp. 77–106, 2015.

[39] M. Cinefra, S. Valvano, and E. Carrera, "A layer-wise MITC9 finite element for the free-vibration analysis of plates with piezo-patches," *International Journal of Smart and Nano Materials*, vol. 6, no. 2, pp. 85–104, 2015.

[40] E. Carrera, "Multilayered shell theories accounting for layerwise mixed description, Part 1: governing equations," *A.I.A.A. J.*, vol. 37, no. 9, pp. 1107–1116, 1999.

[41] E. Carrera, "Multilayered shell theories accounting for layerwise mixed description, Part 2: numerical evaluations," *A.I.A.A. J.*, vol. 37, no. 9, pp. 1117–1124, 1999.

[42] H. Murakami, "Laminated composite plate theory with improved in-plane responses," *J. Appl. Mech.*, vol. 53, pp. 661–666, 1986.

[43] J. N. Reddy, "Mechanics of laminated composite plates and shells," *Theory and Analysis, CRC Press*, 1997.

[44] J. N. Reddy, "An evaluation of equivalent-single-layer and layerwise theories of composite laminates," *Compos. Struct.*, vol. 25, pp. 21–35, 1993.

[45] T. J. R. Hughes, M. Cohen, and M. Horaun, "Reduced and selective integration techniques in the finite element methods," *Nucl. Eng. Des.*, vol. 46, pp. 203–222, 1978.

[46] M. Cinefra and S. Valvano, "A variable kinematic doubly-curved MITC9 shell element for the analysis of laminated composites," *Mech. Adv. Mater. Struc.*, vol. 23, no. 11, pp. 1312–1325, 2016.

[47] M. Cinefra, S. Valvano, and E. Carrera, "Thermal stress analysis of laminated structures by a variable kinematic MITC9 shell element," *J. Therm. Stresses*, vol. 39, no. 2, pp. 121–141, 2016.

[48] V. Tungikar and B. K. M. Rao, "Three dimensional exact solution of thermal stresses in rectangular composite laminates," *Compos. Struct.*, vol. 27, no. 4, pp. 419–430, 1994.

[49] K. Bhaskar, T. K. Varadan, and J. S. M. Ali, "Thermoelastic solutions for orthotropic and anisotropic composite laminates," *Compos. Part B-Eng.*, vol. 27, no. 5, pp. 415–420, 1996.